Quantitative real-time PCR

Quantitative real-time PCR was conducted using the SYBR Green I Master or Probe Master on a LightCycler 480 (Roche). The primer and probe sequences are indicated in Supplementary Table 1. The mRNA of 26 normal tissues was purchased from TAKARA Clontech (Kyoto, Japan).

ChIP assay

Chromatin immunoprecipitation assay was carried out using the CHIP Assay kit (Upstate Biotechnology, Waltham, MA, USA) as previously described (Tanikawa *et al*., 2003). PCR amplifications of *XEDAR* intron 1, containing the consensus p53-binding sites, were performed on immunoprecipitated

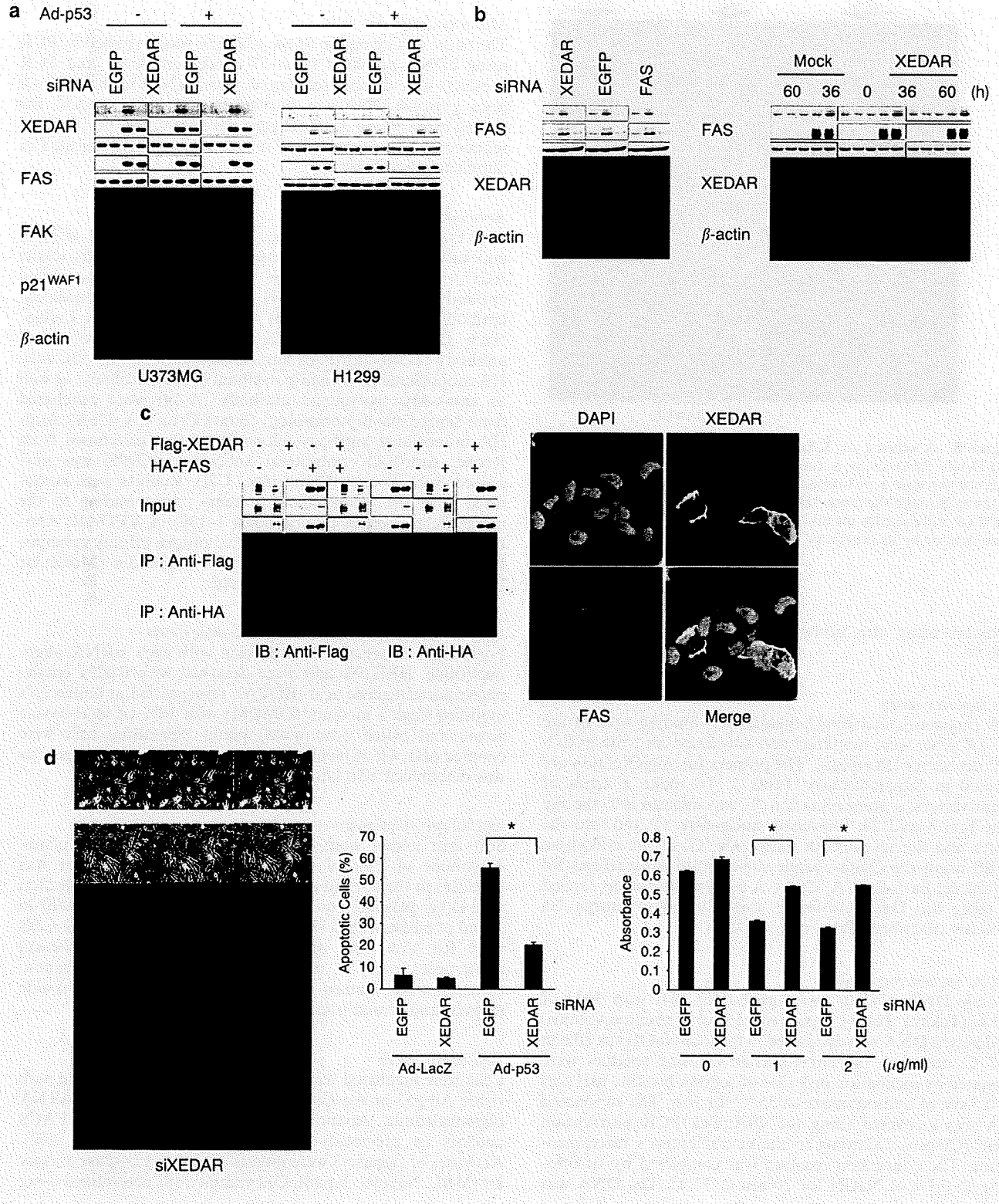

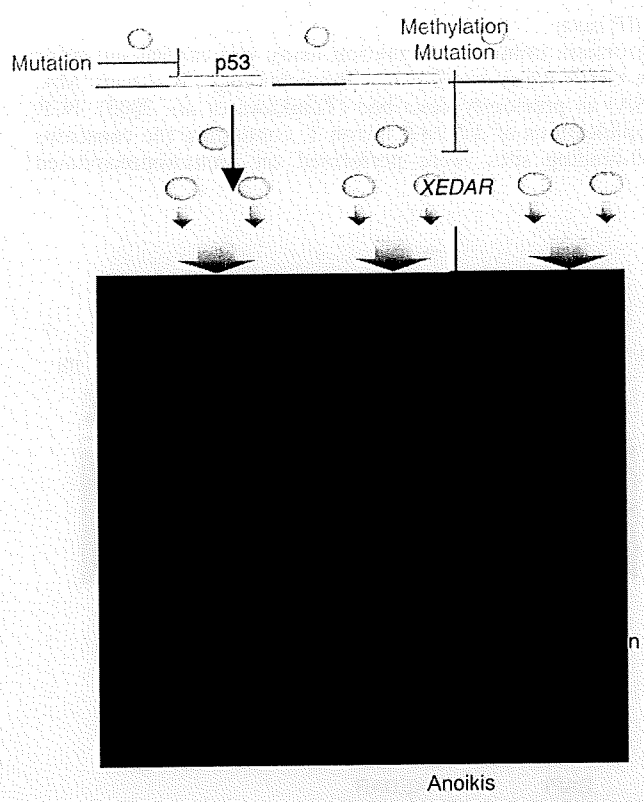

Figure 5 A schema of X-linked ectodermal dysplasia receptor (XEDAR) function as a tumor suppressor gene. *XEDAR* was induced through a p53-dependent manner and mediated anoikis pathway through the cross-talk between FAS and FAK. However, *XEDAR* is frequently inactivated in colorectal cancers by the *p53* mutation, or by its genetic or epigenetic alterations.

chromatin using the primers indicated in Supplementary Table 1.

Gene reporter assay
DNA fragments, including potential p53-binding sites of the *XEDAR* gene, were amplified and subcloned into the pGL3-promoter vector (Promega). The primers for amplification are indicated in Supplementary Table 1. To make a series of mutant vectors, a point mutation 'T' was inserted into the site of the fourth and the fourteenth nucleotide 'C' and into the seventh and the seventeenth nucleotide 'G' of the consensus p53-BS using the QuickChange site-directed mutagenesis kit (Stratagene, La Jolla, CA, USA). A reporter assay was carried out using the Dual Luciferase assay system (Promega) as previously described (Oda *et al*., 2000).

Bisulfite sequencing analysis
Genomic DNA of 3 μg was digested for 16 h with 30 U of *Sau3AI* (Takara, Tokyo, Japan) in a 150 μl of reaction volume. The digested DNA was denatured in 0.3 M of NaOH for 20 min at 37 °C, and then the unmethylated cytosine residues were sulfonated by incubation in 3.12 M of sodium bisulfite (pH 5.0) and 0.5 mM of hydroquinone at 55 °C for 16 h. The sulfonated DNA was recovered using the QIAquick PCR purification system (Qiagen) according to the manufacturer's recommendations. The conversion reaction was completed by desulfonating in 0.3 M of NaOH for 20 min at 37 °C. The DNA was ethanol precipitated and resuspended in double-distilled water. The modified DNA was subjected to PCR amplification of the CpG islands in the *XEDAR* promoter using the primers indicated in Supplementary Table 1. Amplified products were subcloned using the TOPO-TA Cloning System (Invitrogen). Plasmid DNA of at least six insert-positive clones was isolated and sequenced using the ABI sequencing system (Applied Biosystems, Foster City, CA, USA).

Mutation analysis
The entire coding region of the *p53* gene was amplified by PCR using cDNA prepared from 77 cancer cell lines, and PCR products were directly sequenced. For analysis in the *XEDAR* gene, genomic DNA was purified by standard protocol. Six coding exons of the *XEDAR* gene were amplified, purified and sequenced. The primers used in this analysis are indicated in Supplementary Table 1.

Antibodies
Anti-Flag monoclonal (clone M2) and polyclonal (F7425) antibody, as well as anti-β-actin monoclonal antibody (clone AC15) were purchased from Sigma. Anti-p53 monoclonal antibody (Ab-12, clone DO-7) and anti-$p21^{WAF1}$ monoclonal antibody (Ab-1, clone EA10) were purchased from Calbiochem (San Diego, CA, USA). Anti-XEDAR polyclonal antibody (T-14), anti-FAS monoclonal antibody (B-10), anti-HA monoclonal (F-7) and polyclonal (Y-11) antibody, as well as anti-c-Myc polyclonal antibody (A-14) were purchased from Santa Cruz Biotechnology (Santa Cruz, CA, USA). Anti-HA monoclonal antibody (clone 3F10) was purchased from Roche. Anti-FAK polyclonal antibody (ab2999) was purchased from Abcam (Cambridge, UK). Rabbits were immunized with the recombinant proteins corresponding to the extracellular domain (amino acids 1–139) of XEDAR. Antibodies were subsequently purified on antigen affinity columns. For labeling F-actin, Alexa fluor 594 phalloidin (Molecular Probes, Eugene, OR, USA) was used.

Spreading assay and processing morphogenesis
Forty-eight hours after transfection with each siRNA oligonucleotide, HEK293 cells were detached with 0.02% ethylenediaminetetraacetic acid (EDTA), resuspended in Dulbecco's modified Eagle's medium (DMEM) with 10% of fetal bovine serum and plated onto 6-well plates. Spreading cells were counted after 4 h of incubation, and processing morphogenesis was determined 12 h later.

Anchorage-independent growth assay
Soft agar assays were carried out in 6-well culture plates. A volume of 2 ml of culture media with 0.5% agar was solidified in the bottom of each well. At 24 h after transfection with either plasmid, equal numbers of cells were suspended in 1.5 ml of media with 0.33% agar and added to each well. Cells were fed with 1 ml of media supplement with geneticin (Invitrogen) every 3 days. After 2 weeks of incubation, colonies were stained with iodonitrotetrazolium chloride (Sigma) and scored using the Image J software.

Cell death assay
Cells were incubated with adriamycin for 2 h or infected with either Ad-p53 or Ad-LacZ at 6 h after transfection of siRNA oligonucleotide. Apoptotic cells were quantified by FACS analysis as previously described (Matsuda *et al*., 2002). Activities of caspase-3 were monitored using a caspase-3 assay kit (MBL, Nagoya, Japan). Cell viability was determined using

the MTT assay using Cell Counting Kit-8 (Dojindo, Kumamoto, Japan).

Conflict of interest

The authors declare no conflict of interest.

Acknowledgements

We thank T Katagiri for helpful discussion and A Takahashi K Makino for her technical assistance. This work was supported partly by grant #18687012 from Japan Society for the Promotion of Science and Ministry of education, culture, sports, science and technology of Japan (to KM). CT is a JSPS Research Fellow.

References

Afford SC, Randhawa S, Eliopoulos AG, Hubscher SG, Young LS, Adams DH. (1999). CD40 activation induces apoptosis in cultured human hepatocytes via induction of cell surface fas ligand expression and amplifies fas-mediated hepatocyte death during allograft rejection. *J Exp Med* **189**: 441–446.

Beroud C, Soussi T. (2003). The UMD-p53 database: new mutations and analysis tools. *Hum Mutat* **21**: 176–181.

Diez M, Medrano M, Muguerza JM, Ramos P, Hernandez P, Villeta R *et al.* (2000). Influence of tumor localization on the prognostic value of P53 protein in colorectal adenocarcinomas. *Anticancer Res* **20**: 3907–3912.

Folkman J, Moscona A. (1978). Role of cell shape in growth control. *Nature* **273**: 345–349.

Furutani M, Arii S, Tanaka H, Mise M, Niwano M, Harada T *et al.* (1997). Decreased expression and rare somatic mutation of the CIP1/WAF1 gene in human hepatocellular carcinoma. *Cancer Lett* **111**: 191–197.

Golubovskaya VM, Finch R, Kweh F, Massoll NA, Campbell-Thompson M, Wallace MR *et al.* (2008). p53 regulates FAK expression in human tumor cells. *Mol Carcinog* **47**: 373–382.

Grell M, Zimmermann G, Gottfried E, Chen CM, Grunwald U, Huang DC *et al.* (1999). Induction of cell death by tumour necrosis factor (TNF) receptor 2, CD40 and CD30: a role for TNF-R1 activation by endogenous membrane-anchored TNF. *EMBO J* **18**: 3034–3043.

Hollstein M, Rice K, Greenblatt MS, Soussi T, Fuchs R, Sorlie T *et al.* (1994). Database of p53 gene somatic mutations in human tumors and cell lines. *Nucleic Acids Res* **22**: 3551–3555.

Ilic D, Almeida EA, Schlaepfer DD, Dazin P, Aizawa S, Damsky CH. (1998). Extracellular matrix survival signals transduced by focal adhesion kinase suppress p53-mediated apoptosis. *J Cell Biol* **143**: 547–560.

Ilic D, Furuta Y, Kanazawa S, Takeda N, Sobue K, Nakatsuji N *et al.* (1995). Reduced cell motility and enhanced focal adhesion contact formation in cells from FAK-deficient mice. *Nature* **377**: 539–544.

Kidokoro T, Tanikawa C, Furukawa Y, Katagiri T, Nakamura Y, Matsuda K. (2008). CDC20, a potential cancer therapeutic target, is negatively regulated by p53. *Oncogene* **27**: 1562–1571.

Kitahara O, Furukawa Y, Tanaka T, Kihara C, Ono K, Yanagawa R *et al.* (2001). Alterations of gene expression during colorectal carcinogenesis revealed by cDNA microarrays after laser-capture microdissection of tumor tissues and normal epithelia. *Cancer Res* **61**: 3544–3549.

Lark AL, Livasy CA, Calvo B, Caskey L, Moore DT, Yang X *et al.* (2003). Overexpression of focal adhesion kinase in primary colorectal carcinomas and colorectal liver metastases: immunohistochemistry and real-time PCR analyses. *Clin Cancer Res* **9**: 215–222.

Lee SH, Shin MS, Kim HS, Lee HK, Park WS, Kim SY *et al.* (1999). Alterations of the DR5/TRAIL receptor 2 gene in non-small cell lung cancers. *Cancer Res* **59**: 5683–5686.

Levine AJ. (1997). p53, the cellular gatekeeper for growth and division. *Cell* **88**: 323–331.

Liang F, Liang J, Wang WQ, Sun JP, Udho E, Zhang ZY. (2007). PRL3 promotes cell invasion and proliferation by down-regulation of Csk leading to Src activation. *J Biol Chem* **282**: 5413–5419.

Liu X, Yue P, Khuri FR, Sun SY. (2005). Decoy receptor 2 (DcR2) is a p53 target gene and regulates chemosensitivity. *Cancer Res* **65**: 9169–9175.

Matsuda K, Yoshida K, Taya Y, Nakamura K, Nakamura Y, Arakawa H. (2002). p53AIP1 regulates the mitochondrial apoptotic pathway. *Cancer Res* **62**: 2883–2889.

McLean GW, Carragher NO, Avizienyte E, Evans J, Brunton VG, Frame MC. (2005). The role of focal-adhesion kinase in cancer—a new therapeutic opportunity. *Nat Rev Cancer* **5**: 505–515.

Mori T, Anazawa Y, Iiizumi M, Fukuda S, Nakamura Y, Arakawa H. (2002). Identification of the interferon regulatory factor 5 gene (IRF-5) as a direct target for p53. *Oncogene* **21**: 2914–2918.

Naito A, Yoshida H, Nishioka E, Satoh M, Azuma S, Yamamoto T *et al.* (2002). TRAF6-deficient mice display hypohidrotic ectodermal dysplasia. *Proc Natl Acad Sci USA* **99**: 8766–8771.

Nakamura Y. (2004). Isolation of p53-target genes and their functional analysis. *Cancer Sci* **95**: 7–11.

Newton K, French DM, Yan M, Frantz GD, Dixit VM. (2004). Myodegeneration in EDA-A2 transgenic mice is prevented by XEDAR deficiency. *Mol Cell Biol* **24**: 1608–1613.

Nikiforov MA, Hagen K, Ossovskaya VS, Connor TM, Lowe SW, Deichman GI *et al.* (1996). p53 modulation of anchorage independent growth and experimental metastasis. *Oncogene* **13**: 1709–1719.

Oda K, Arakawa H, Tanaka T, Matsuda K, Tanikawa C, Mori T *et al.* (2000). p53AIP1, a potential mediator of p53-dependent apoptosis, and its regulation by Ser-46-phosphorylated p53. *Cell* **102**: 849–862.

Owens LV, Xu L, Craven RJ, Dent GA, Weiner TM, Kornberg L *et al.* (1995). Overexpression of the focal adhesion kinase (p125FAK) in invasive human tumors. *Cancer Res* **55**: 2752–2755.

Pharoah PD, Day NE, Caldas C. (1999). Somatic mutations in the p53 gene and prognosis in breast cancer: a meta-analysis. *Br J Cancer* **80**: 1968–1973.

Rampino N, Yamamoto H, Ionov Y, Li Y, Sawai H, Reed JC *et al.* (1997). Somatic frameshift mutations in the BAX gene in colon cancers of the microsatellite mutator phenotype. *Science* **275**: 967–969.

Sinha SK, Chaudhary PM. (2004). Induction of apoptosis by X-linked ectodermal dysplasia receptor via a caspase 8-dependent mechanism. *J Biol Chem* **279**: 41873–41881.

Sinha SK, Zachariah S, Quinones HI, Shindo M, Chaudhary PM. (2002). Role of TRAF3 and -6 in the activation of the NF-kappa B and JNK pathways by X-linked ectodermal dysplasia receptor. *J Biol Chem* **277**: 44953–44961.

Smahi A, Courtois G, Rabia SH, Doffinger R, Bodemer C, Munnich A *et al.* (2002). The NF-kappaB signalling pathway in human diseases: from incontinentia pigmenti to ectodermal dysplasias and immune-deficiency syndromes. *Hum Mol Genet* **11**: 2371–2375.

Takakuwa T, Dong Z, Nakatsuka S, Kojya S, Harabuchi Y, Yang WI *et al.* (2002). Frequent mutations of Fas gene in nasal NK/T cell lymphoma. *Oncogene* **21**: 4702–4705.

Tanaka H, Arakawa H, Yamaguchi T, Shiraishi K, Fukuda S, Matsui K *et al.* (2000). A ribonucleotide reductase gene involved in

a p53-dependent cell-cycle checkpoint for DNA damage. *Nature* **404**: 42–49.

Tanikawa C, Matsuda K, Fukuda S, Nakamura Y, Arakawa H. (2003). p53RDL1 regulates p53-dependent apoptosis. *Nat Cell Biol* **5**: 216–223.

Vogelstein B, Fearon ER, Kern SE, Hamilton SR, Preisinger AC, Nakamura Y *et al.* (1989). Allelotype of colorectal carcinomas. *Science* **244**: 207–211.

Vogelstein B, Lane D, Levine AJ. (2000). Surfing the p53 network. *Nature* **408**: 307–310.

Weiner TM, Liu ET, Craven RJ, Cance WG. (1993). Expression of focal adhesion kinase gene and invasive cancer. *Lancet* **342**: 1024–1025.

Wu GS, Burns TF, McDonald III ER, Jiang W, Meng R, Krantz ID *et al.* (1997). KILLER/DR5 is a DNA damage-inducible p53-regulated death receptor gene. *Nat Genet* **17**: 141–143.

Yan M, Wang LC, Hymowitz SG, Schilbach S, Lee J, Goddard A *et al.* (2000). Two-amino acid molecular switch in an epithelial morphogen that regulates binding to two distinct receptors. *Science* **290**: 523–527.

Supplementary Information accompanies the paper on the Oncogene website (http://www.nature.com/onc)

Vol 461|10 September 2009|doi:10.1038/nature08283

ARTICLES

An RNA-dependent RNA polymerase formed by TERT and the *RMRP* RNA

Yoshiko Maida[1], Mami Yasukawa[1], Miho Furuuchi[1], Timo Lassmann[2], Richard Possemato[3], Naoko Okamoto[1], Vivi Kasim[1], Yoshihide Hayashizaki[2], William C. Hahn[3,4] & Kenkichi Masutomi[1,5]

Constitutive expression of telomerase in human cells prevents the onset of senescence and crisis by maintaining telomere homeostasis. However, accumulating evidence suggests that the human telomerase reverse transcriptase catalytic subunit (TERT) contributes to cell physiology independently of its ability to elongate telomeres. Here we show that TERT interacts with the RNA component of mitochondrial RNA processing endoribonuclease (*RMRP*), a gene that is mutated in the inherited pleiotropic syndrome cartilage–hair hypoplasia. Human TERT and *RMRP* form a distinct ribonucleoprotein complex that has RNA-dependent RNA polymerase (RdRP) activity and produces double-stranded RNAs that can be processed into small interfering RNA in a Dicer (also known as DICER1)-dependent manner. These observations identify a mammalian RdRP composed of TERT in complex with *RMRP*.

Telomerase is a ribonucleoprotein complex that elongates telomeres. Although several proteins interact with telomerase[1–4], the minimal components of active telomerase include the catalytic telomerase reverse transcriptase (TERT) and a noncoding RNA (*TERC*) that encodes the template to synthesize telomeric DNA[5]. Telomere homeostasis mediated by telomerase maintains genomic stability and regulates cell lifespan[6]. Mutations in TERT, *TERC* or dyskerin, a telomerase-associated nucleolar protein involved in ribosomal RNA maturation[7], are found in dyskeratosis congenita, a syndrome characterized by ectodermal dysplasia and bone marrow failure, and TERT mutations have been reported in aplastic anaemia and idiopathic pulmonary fibrosis[8]. Moreover, alterations in the regulation of telomeres and telomerase contribute to malignant transformation by affecting genomic integrity and cell immortalization[6].

However, accumulating evidence suggests that TERT has activities beyond telomere maintenance[9–13] and forms several intracellular complexes[2–4]. In particular, the overexpression of TERT induces increased tumour susceptibility[9,10] and disrupts stem-cell function independently of telomere maintenance[12], whereas the suppression of TERT expression alters global chromatin structure[11]. Indeed, some of these telomere-independent functions of TERT do not require the expression of *TERC*[12].

Identification of a second RNA that interacts with TERT

To identify human TERT partners, we stably overexpressed a tandem affinity peptide (TAP)-tagged TERT protein in HeLa S3 cells, isolated TERT immune complexes, and identified a heterogeneous mixture of 38 RNA sequences associated with TERT (Supplementary Fig. 2 and Supplementary Table 1). We found that 5% of the sequences corresponded to *TERC* and the RNA component of mitochondrial RNA processing endoribonuclease (*RMRP*). *RMRP* is a 267-nucleotide noncoding RNA that is a small nucleolar RNA, like *TERC*, and is also found in mitochondria[8,14]. *RMRP* mutations are found in the pleiotropic inherited syndrome, cartilage–hair hypoplasia[15].

From a single immune complex, we confirmed that either overexpressed or endogenous TERT interacts with *RMRP* and *TERC*, by isolating TAP–TERT (Fig. 1a) or endogenous TERT (Fig. 1b) complexes in both HeLa and 293T cells under conditions in which we failed to recover the ribozyme *RNase P*. We also found that the abundance of TERT–*RMRP* and TERT–*TERC* complexes was similar, even though *TERC* was expressed at five-fold higher levels than *RMRP* in these cells (Fig. 1c and Supplementary Fig. 3).

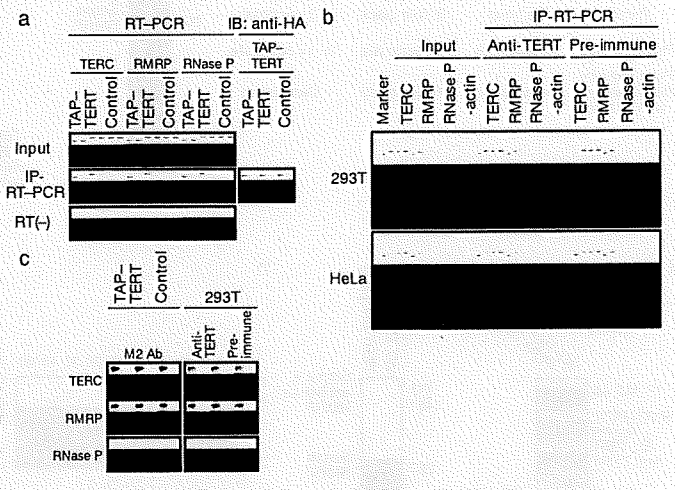

Figure 1 | TERT and *RMRP* interact. a, Detection of *RMRP* and *TERC*. RNA species associated with TAP–TERT complexes from a single immunoprecipitation (IP) were isolated and subjected to PCR with reverse transcription (RT–PCR). RT (−) indicates the absence of reverse transcriptase. Right panel shows the levels of TAP–TERT. HA, haemagglutinin; IB, immunoblot. **b**, TERT interacts with endogenous *RMRP*. TERT complexes from 293T and HeLa cells were isolated with an anti-TERT antibody and associated RNAs were subjected to RT–PCR. **c**, RNAs purified from TERT complexes isolated from HeLa S3 cells expressing TAP–TERT or a control vector or 293T cells were subjected to northern blotting. Ab, antibody.

[1]Cancer Stem Cell Project, National Cancer Center Research Institute, 5-1-1 Tsukiji, Chuo-ku, Tokyo 104-0045, Japan. [2]RIKEN Omics Science Center, RIKEN Yokohama Institute, 1-7-22 Suehiro-cho, Tsurumi-ku, Yokohama 230-0045, Japan. [3]Department of Medical Oncology, Dana-Farber Cancer Institute and Departments of Medicine, Brigham and Women's Hospital and Harvard Medical School, 44 Binney Street, Boston, Massachusetts 02115, USA. [4]Broad Institute of Harvard and MIT, 7 Cambridge Center, Cambridge, Massachusetts 02142, USA. [5]PREST, Japan Science and Technology Agency, 4-1-8 Honcho Kawaguchi, Saitama 332-0012, Japan.

To characterize the interaction between TERT and *RMRP*, we used TERT truncation mutants and found that the amino terminal end of TERT (1–531) was necessary for interactions with *RMRP* (Supplementary Fig. 4). This region overlaps with two regions required for the binding of *TERC*[8,16]. These observations demonstrate that TERT and *RMRP* form a new ribonucleoprotein complex distinct from the TERT–*TERC* enzyme.

The TERT–*RMRP* complex has RdRP activity

To test whether *RMRP* substitutes for *TERC* to reconstitute telomerase activity, we combined recombinant TERT with *TERC* or *RMRP* RNAs transcribed *in vitro*. Although we detected telomerase activity with TERT and *TERC* (Supplementary Fig. 5), we failed to detect telomerase activity when TERT and *RMRP* were co-incubated.

TERT has also been shown to act as a terminal transferase[17], and human TERT shares sequence similarity to both viral reverse transcriptases and RdRPs[18]. RdRPs participate in the endogenous RNA interference (RNAi) pathway and in the regulation of post-transcriptional gene silencing[19–23]. To examine whether the TERT–*RMRP* complex has RdRP and/or terminal transferase activity, we established an RNA synthesis activity assay with recombinant TERT protein (Supplementary Fig. 6) and RNA molecules transcribed *in vitro*. We predicted three modes that the TERT–*RMRP* complex might use to elongate RNA: (1) as an RdRP that uses a *de-novo*-synthesized RNA primer to elongate a complementary strand (Fig. 2a, left panel); (2) as an RdRP that uses a 3′ fold-back (back-priming) configuration of template RNA as a primer (Fig. 2a, middle panel); or (3) as a terminal transferase (Fig. 2a, right panel). Viral RdRPs[24,25] have been shown to use the first two modes to prime RdRP activity, and cellular RdRPs in fission yeast[26] and fungi[23] use similar priming mechanisms to produce double-stranded (ds) RNAs that act as precursors for RNAi.

We found that recombinant TERT and *RMRP* produced two different products depending on the salt concentration (Fig. 2b and Supplementary Fig. 7). Specifically, we found ~267-nucleotide-(corresponding to sense *RMRP*) and ~534-nucleotide-sized products (hereafter referred to as sense plus antisense *RMRP* products) under high salt conditions, and *RMRP*-sized products under low salt conditions. To discriminate between these modes, we treated the products of the RdRP assay with RNase T1 (Fig. 2c) using conditions that favour the digestion of single-stranded RNA. RNase T1 treatment eliminated the ~267-nucleotide *RMRP*-sized RNA products produced under low salt concentrations (data not shown), indicating that [^{32}P]UTP was incorporated by terminal transferase activity.

In contrast, under high salt conditions, we found two RNAs (~267 and ~534 nucleotides) that collapsed into a single ~267-nucleotide band after treatment with RNase T1 (Fig. 2c). To eliminate the possibility that the sense plus antisense product represented partially denatured RNAs, we treated the products of the RdRP assay with bacterial RNase III to digest dsRNA, and found that only the input ~267-nucleotide RNA remained (Fig. 2d). Furthermore, when we left out adenine or guanine ribonucleotides, we failed to detect the sense plus antisense product (Fig. 2e). These observations confirm that the ~534-nucleotide sense plus antisense products are formed by RdRP activity and represent a double-stranded hairpin structure created by an RNA molecule composed of sense and antisense strands of *RMRP*.

To confirm that the interaction between TERT and *RMRP* was required for RdRP activity, we performed an RdRP activity assay using

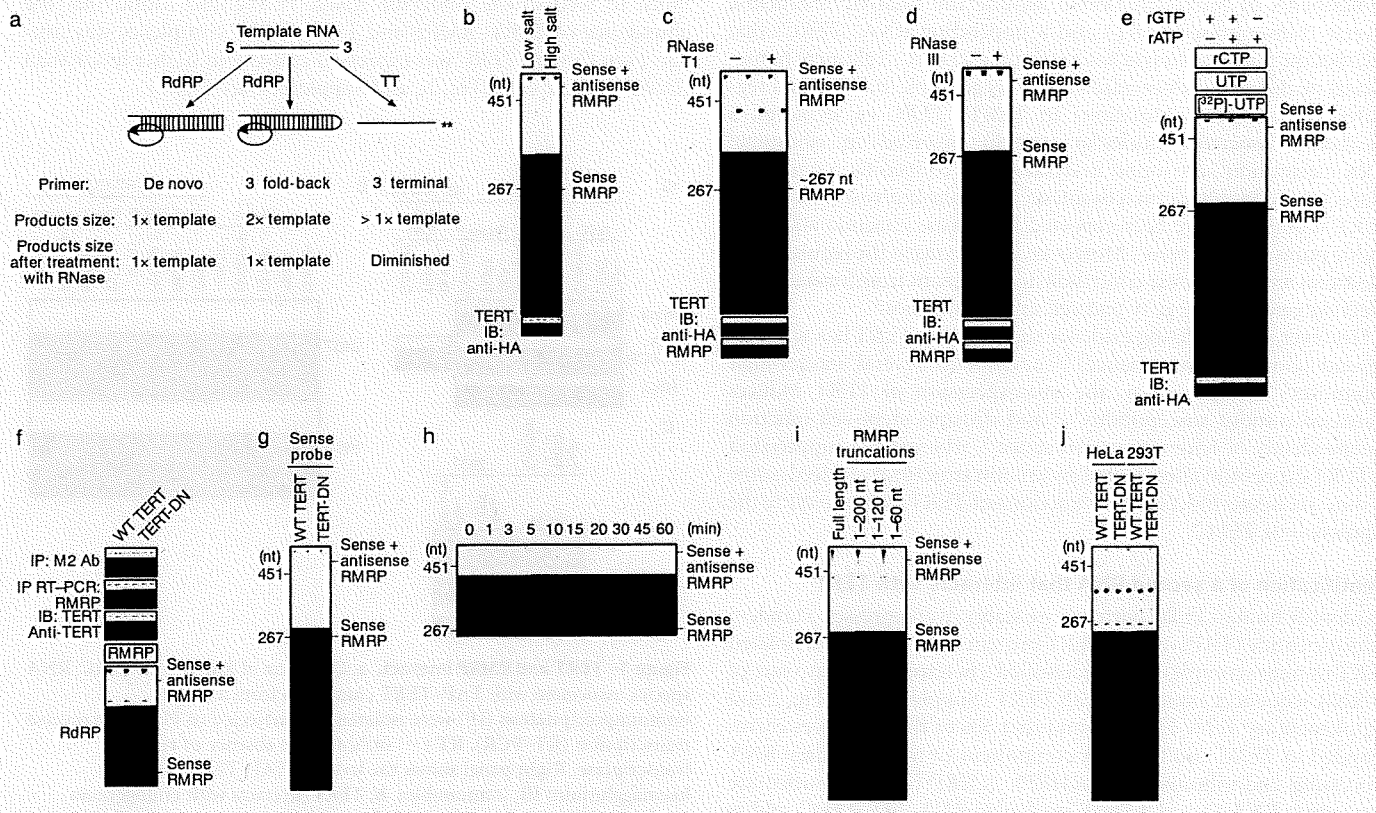

Figure 2 | TERT and *RMRP* have RdRP activity. **a**, Predicted RNA products produced by RdRP or terminal transferase (TT) activity. **b**, RNA products produced by the RdRP activity derived from recombinant TERT and *RMRP*. nt, nucleotides. **c**, **d**, Treatment of RNA products with RNase T1 (**c**) or bacterial RNase III (**d**). **e**, RdRP assay performed in the presence of ribonucleotides (middle) or in the absence of adenine (left lane) or guanine (right lane) ribonucleotides. A and G are present within the first 5 nucleotides of the predicted complementary strand of *RMRP*. **f**, TERT-DN binds *RMRP* but lacks RdRP activity. TERT immune complexes were isolated from 293T cells expressing Flag-tagged TERT or Flag-tagged TERT-DN. RdRP activity is shown in the bottom panel. WT, wild-type. **g**, Northern blotting to detect complementary sequence of *RMRP*. **h**, Time course of RdRP activity. **i**, RNA products produced by recombinant TERT and truncation mutants of *RMRP* transcribed *in vitro*. Faint signals at 200, 120 and 60 nucleotides are TERT terminal transferase products. **j**, RNA products produced by the RdRP activity derived from recombinant TERT or TERT-DN and total RNA. A limited pool of RNAs serves as template for RdRP activity.

combinations of recombinant mutant TERT proteins and *RMRP*. We failed to detect RdRP reaction products when TERT and *TERC* were co-incubated (Supplementary Fig. 8). Moreover, when we used the TERT-HT1 mutant that does not bind *RMRP* (Supplementary Fig. 4), we failed to observe labelled RNA products (Supplementary Fig. 8) under conditions in which we detected two different RNA products in reactions containing wild-type TERT and *RMRP*. We previously described a catalytically inactive TERT mutant (TERT-DN) that fails to elongate telomeres[11,27]. We confirmed that the recombinant TERT-DN mutant retained the ability to bind *RMRP* (Fig. 2f), but that the TERT-DN–*RMRP* complex lacked detectable RdRP activity (Fig. 2f). Thus TERT acts as the catalytic subunit for both the telomerase reverse transcriptase and RdRP activities.

TERT–*RMRP* RdRP produces dsRNA

These observations suggest that the TERT–*RMRP* RdRP synthesizes dsRNA in a template-dependent manner. To confirm the synthesis of the *RMRP* complementary strand, we used the sense strand of *RMRP* as a probe in northern blotting. We detected the antisense strand of *RMRP* in reactions containing recombinant wild-type TERT protein and *RMRP*, but not in reactions containing TERT-DN and *RMRP* (Fig. 2g). Furthermore, we detected the sense plus antisense product in the RdRP assay using the antisense strand of *RMRP* as a probe (Supplementary Fig. 9). These observations indicate that the TERT–*RMRP* RdRP produces dsRNAs in a template-dependent manner *in vitro*.

To determine whether the TERT–*RMRP* RdRP uses a back-priming mechanism, we examined the priming process using TERT and *RMRP* as a model system and found that elongation products appeared in a time-dependent manner (Fig. 2h and Supplementary Fig. 10). To assess whether the *RMRP* RNA forms a 3′ fold-back configuration, we generated 3′ *RMRP* truncation mutants and failed to find any reaction products (Fig. 2i). Thus, unlike what has been described for other cellular RdRPs, the TERT–*RMRP* RdRP has a restricted preference for RNA molecules that can be used as a template. Indeed, when we incubated purified recombinant TERT together with total cellular RNA and [^{32}P]UTP, we identified a limited number of labelled RNAs (Fig. 2j). Although the secondary structure adopted by *RMRP* to create the 3′ fold-back is not known, these observations suggest that *RMRP* can itself serve as a primer for the polymerization process using a 3′ fold-back structure.

To ascertain whether this RdRP activity also occurs *in vivo*, we used the sense strand of *RMRP* as a probe and found ~534-nucleotide RNAs that contain antisense *RMRP* in RNA derived from 293T, HeLa and MCF7 cells (Fig. 3a and Supplementary Figs 11 and 12). Moreover, we detected sense products and sense plus antisense products using *RMRP* antisense-strand probe (Fig. 3b). These observations confirmed that the ~534-nucleotide products contain both sense and antisense *RMRP* sequences. To determine whether TERT was necessary for the appearance of antisense *RMRP* in cells, we examined the levels of the complementary *RMRP* strand in cells that do not express TERT and *TERC* (VA-13 cells)[28], in cells that transiently express low levels of TERT (BJ cells)[27,29,30], and in cells that constitutively express TERT (293T and HeLa cells). We also introduced a control vector or a vector that encodes TERT in VA-13 and BJ cells. We detected the complementary *RMRP* strand using a quantitative RNase protection assay with a sense-strand probe that detects antisense *RMRP* (Fig. 3c and Supplementary Fig. 13), and using northern blotting with both sense and antisense strand-specific *RMRP* probes (Fig. 3d and Supplementary Fig. 11a). The levels of antisense *RMRP* correlated with the expression of TERT (Fig. 3c, d). These observations confirmed that the TERT–*RMRP* RdRP produces double-stranded *RMRP in vivo*.

Effects of the TERT–*RMRP* complex on *RMRP* expression

To assess the consequences of overexpressing the TERT–*RMRP* complex on *RMRP* levels, we introduced *RMRP* into cells that lack TERT

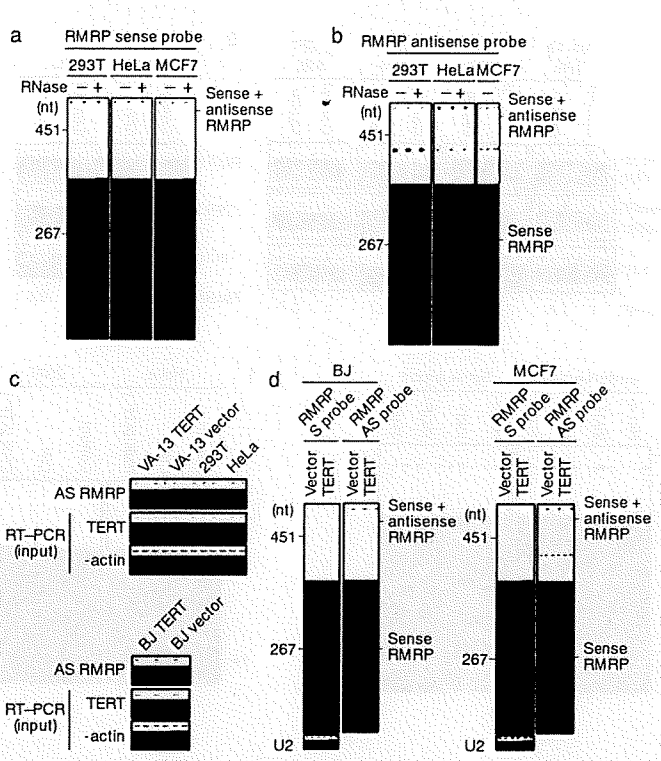

Figure 3 | Identification of dsRNA synthesized by the TERT–*RMRP* RdRP. **a**, Northern blotting to detect complementary sequence of *RMRP* in cell lines. '+' indicates samples treated with RNase. **b**, Northern blotting to detect the *RMRP* sense strand. **c**, TERT expression correlates with the levels of antisense (AS) *RMRP* detected by RNase protection assay. Vector denotes cells infected with a control vector. **d**, TERT expression correlates with the levels of the sense (S) plus antisense *RMRP* products detected by northern blotting. The bottom panel shows levels of the small nuclear RNA *U2*.

expression (VA-13), that transiently express TERT in a cell-cycle-dependent manner (BJ fibroblasts), and that constitutively express TERT (VA-13 and BJ fibroblasts expressing ectopic TERT, and HeLa and MCF7 cells). After expressing *RMRP* in cells lacking TERT (VA-13), we found that *RMRP* levels were increased (Fig. 4a and Supplementary Fig. 14). In contrast, in cells that express TERT, we found that the steady-state levels of *RMRP* were decreased when *RMRP* was overexpressed, regardless of the promoter that was used to express *RMRP* (Fig. 4a and Supplementary Fig. 14). We also found that forced TERT expression in VA-13 or BJ cells suppressed *RMRP* expression (Fig. 4b and Supplementary Fig. 15). Consistent with these findings, suppression of TERT in HeLa cells led to increased *RMRP* expression (Fig. 4c).

Because the 3′ end of *RMRP* was essential for TERT–*RMRP* activity (Fig. 2i), we examined the effects of expressing *RMRP* truncation mutants lacking 3′ ends and found that only truncation mutants lacking intact 3′ ends were readily overexpressed (Fig. 4d). These observations demonstrate that *RMRP* expression levels are dependent on the TERT–*RMRP* RdRP and suggest that *RMRP* levels are controlled by an RdRP-dependent, negative-feedback mechanism.

Identification of siRNAs derived from *RMRP*

In other organisms, RdRPs synthesize dsRNAs that are processed into active short interfering RNAs (siRNAs)[31]. Because manipulating TERT and *RMRP* levels affected *RMRP* expression, we proposed that the TERT–*RMRP* complex produces *RMRP*-specific siRNA to regulate *RMRP* levels. To test this possibility, we used sense and antisense probes corresponding to *RMRP* (nucleotides 21–40) in northern blotting and found double-stranded 22-nucleotide RNAs (Fig. 4e and Supplementary Fig. 11b). Because siRNAs contain 5′ monophosphate and 3′ hydroxyl groups[32–34], we characterized the chemical

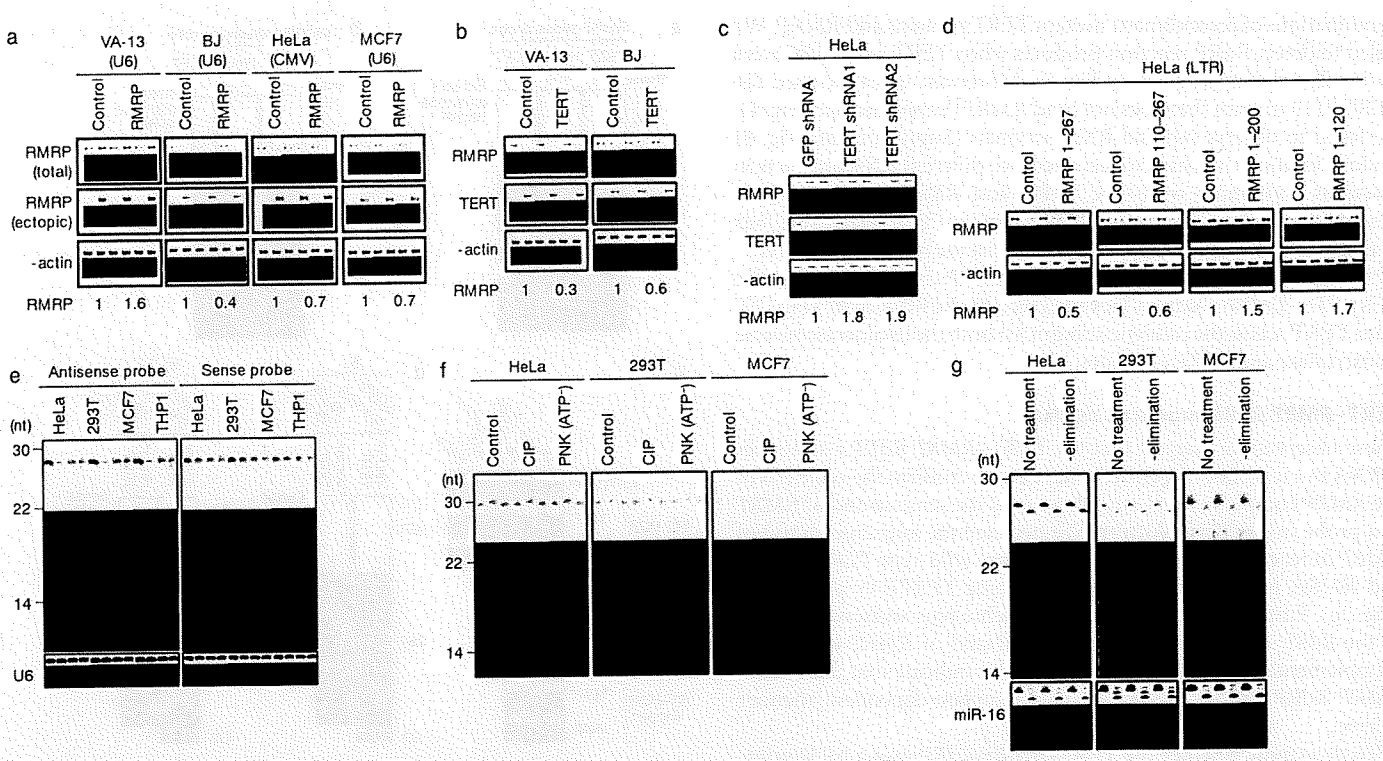

Figure 4 | Effects of dsRNA produced by the TERT–*RMRP* RdRP. **a**, Semi-quantitative RT–PCR for total *RMRP* and retrovirally delivered *RMRP* (ectopic) in cell lines expressing control or *RMRP* expression vectors. Promoters used to express *RMRP* are indicated. The relative intensity of *RMRP* is noted below each panel. CMV, cytomegalovirus. See Supplementary Fig. 14. **b**, RT–PCR for total *RMRP*. See Supplementary Fig. 15. **c**, Effects of suppressing TERT on *RMRP* levels. A control shRNA (green fluorescent protein (GFP) shRNA) or two different *TERT*-specific shRNAs were stably introduced into HeLa cells. **d**, Effects of *RMRP* mutants on *RMRP* levels. LTR, long terminal repeat. RT–PCR was used to detect *RMRP* levels in **c** and **d**. **e**, Detection of small RNA species in human cells. Northern blotting to detect small RNAs (22 nucleotides in length) using antisense (left panel) and sense (right panel) probes derived from nucleotides 21–40 of *RMRP*. **f**, **g**, Analysis of the termini of the small RNA species identified in **e**. Total RNA was incubated with the indicated enzyme (**f**), or oxidation-β-elimination reactions (**g**) were performed. Northern blotting was performed with antisense probe. CIP, calf intestinal phosphatase; PNK, polynucleotide kinase. ATP- indicates samples lacking ATP.

nature of the small RNA ends. We found that calf intestinal phosphatase slowed the migration of these short RNAs, and subsequent incubation with polynucleotide kinase and ATP restored the mobility of the short RNAs, indicating that either the 5′ or the 3′ end of this small RNA is monophosphorylated (Fig. 4f and data not shown). Moreover, incubation with polynucleotide kinase in the absence of ATP did not alter the migration (Fig. 4f), and oxidation and β-elimination treatment increased the migration of these small RNAs (Fig. 4g), indicating that the 3′ ends bear vicinal 2′,3′ dihydroxyls. Together, these observations confirm that these small RNAs contain 5′ monophosphate and 3′ hydroxyl groups, and therefore share the size and chemical composition of known siRNAs.

To demonstrate that dsRNAs produced by the TERT–*RMRP* RdRP are processed into siRNA, we suppressed the expression of *Dicer* with two distinct *Dicer*-specific short hairpin RNAs (shRNAs). Suppression of *Dicer* to levels that partially inhibited the processing of the microRNA *miR-16* (Fig. 5a and Supplementary Fig. 16) led to diminished levels of the siRNAs derived from *RMRP* (Fig. 5a). When we suppressed *Dicer* expression in HeLa, 293T or MCF7 cells, we found that endogenous *RMRP* levels increased up to 3.7-fold (Fig. 5b). Suppressing *Dicer* expression in VA-13 cells that lack TERT did not affect the levels of single-stranded *RMRP* (Fig. 5b), but did increase levels of the elongated sense plus antisense *RMRP* products in cells that constitutively express TERT (Supplementary Fig. 17). Moreover, we found that only the sense strands of these endogenous *RMRP*-specific siRNAs were associated with human AGO2 (also known as EIF2C2; Fig. 5c). These observations indicate that the endogenous *RMRP*-specific siRNAs are processed by the RNA-induced silencing complex, similar to other small RNAs that are processed into siRNA.

To confirm that these small RNAs act as siRNAs, we identified small RNAs from total RNA that hybridized to probes spanning *RMRP*, synthesized siRNA corresponding to the identified sequences, and tested the consequences of introducing this siRNA in HeLa, 293T and MCF7 cells. We found that the synthesized siRNA suppressed endogenous *RMRP* levels (Supplementary Fig. 18). These observations provide evidence that similar to other cellular RdRPs, the TERT–*RMRP* RdRP synthesizes dsRNAs that act as a precursor for siRNAs.

Discussion

Here we demonstrate that human TERT and *RMRP* form a distinct ribonucleoprotein complex that has the ability to produce dsRNAs (Supplementary Fig. 1). Like RdRPs found in other organisms, the human TERT–*RMRP* complex produces dsRNAs that act as substrates for the generation of siRNA. However, unlike other cellular RdRPs[23,26,31,35,36], the human TERT–*RMRP* RdRP shows a strong preference for RNA templates that can form 3′ fold-back structures. Because other cellular RdRPs have been identified using assays that require primer-independent RdRP activity[23,26,36], the substrate specificity of the human TERT–*RMRP* RdRP may, in part, account for the difficulty in identifying mammalian enzymes that have RdRP activity.

Although the cellular RdRPs described until now do not show a primer requirement, several viral RdRPs use both primer-dependent and primer-independent mechanisms, and fungal and yeast RdRPs are also able to use a back-priming mechanism[23,26]. Because TERT is a closed right-handed polymerase[37] evolutionarily related to both reverse transcriptases and viral RdRPs[18], these observations are consistent with previous observations that indicate that right-handed RdRPs exhibit primer-dependent RdRP polymerase activity[38].

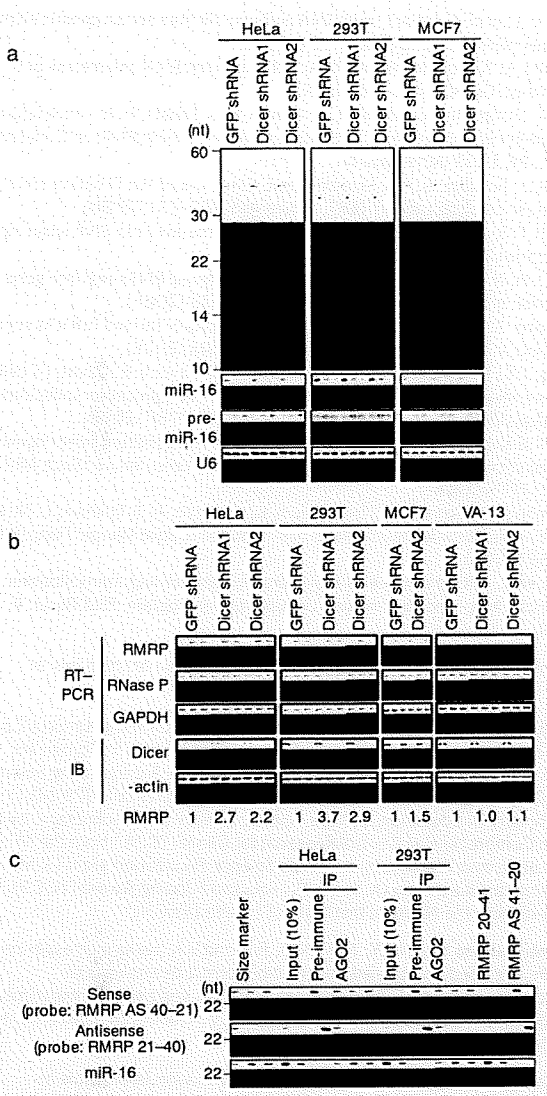

Figure 5 | Production of *RMRP*-derived endogenous siRNAs depends on Dicer. a, Effect of suppressing *Dicer* on *RMRP*-derived small RNAs. Northern blotting was performed to detect: (1) small RNAs using the antisense strand of *RMRP* as a probe in the indicated cells expressing control shRNA (GFP shRNA) or *Dicer*-specific shRNAs (*Dicer* shRNA1 and shRNA2); (2) precursor microRNA *pre-miR-16* and mature *miR-16* using a *miR-16*-specific probe; and (3) *U6* RNA. See Supplementary Fig. 16. **b**, RT–PCR for total *RMRP* from cell lines expressing control shRNA or *Dicer*-specific shRNAs. IB, immunoblot. The relative intensity of *RMRP* is noted at the bottom of the panel. **c**, *RMRP*-derived small RNAs are associated with AGO2. Human AGO2 immune complexes were isolated using anti-AGO2-specific antisera or pre-immune sera, and small RNAs were detected by northern blotting. Blotting of oligonucleotides (*RMRP* 20–41 and *RMRP* AS 41–20) is also shown.

Using *RMRP* as a template, the TERT–*RMRP* RdRP produces dsRNAs that are processed by Dicer into 22-nucleotide dsRNAs that contain 5′ monophosphate and 3′ hydroxyl groups and are loaded into AGO2, confirming that these short RNAs represent endogenous siRNAs. Recent work has shown that in oocytes and embryonic stem cells, endogenous siRNA can also be formed by the transcription of complementary sense and antisense strands[39–41]. Thus, in mammals at least two mechanisms lead to the production of dsRNAs that are processed into siRNA. Further work will be necessary to determine whether there are tissue-dependent differences in the use of these two mechanisms and whether other mammalian RdRPs exist.

We found that the TERT–*RMRP* RdRP regulates *RMRP* levels by a negative-feedback control mechanism. The identities and functions of the RNAs other than *RMRP* that act as templates for the TERT–*RMRP* RdRP remain to be identified (Fig. 2j). However, because endogenously encoded siRNAs suppress L1 retrotransposition in human cells[42], these observations suggest that the TERT–*RMRP* complex may regulate the expression of other genes by generating siRNAs.

Because mutations in *RMRP* are found in cartilage–hair hypoplasia[15], these findings suggest that perturbation of the TERT–*RMRP* complex is involved in the pathogenesis of this disorder. The involvement of human TERT in two syndromes characterized by stem-cell failure (cartilage–hair hypoplasia and dyskeratosis congenita)[7,8,43] suggests that ribonucleoprotein complexes containing TERT has a critical role in stem cell biology. Indeed, overexpression of mouse TERT in mice lacking *Terc* leads to defects in normal hair follicle stem-cell function[12] at least in part by altering gene expression programs related to stem cell function[44]. In mammals, TERT may regulate both telomere biology and gene expression through these two ribonucleoprotein complexes.

METHODS SUMMARY

RNAs that bind TERT were identified from HeLa S3 cells expressing a TAP epitope-tagged TERT. RNAs that bound to TERT after two rounds of purification were analysed using an Experion capillary electrophoresis device (Bio-Rad) to visualize RNA species. For RNA cloning and sequencing, the same samples were separated using a 7 M urea/15% polyacrylamide gel, and RNAs recovered from the gel were cloned using a small RNA cloning Kit (TaKaRa). Purified glutathione *S*-transferase (GST)–TERT was isolated from *Escherichia coli* and incubated with either *TERC* or *RMRP* transcribed *in vitro*, to assess the ability of such complexes to exhibit telomerase or RdRP activity. RNAi was used to suppress TERT and to show that the TERT–*RMRP* complex also produces dsRNA in cells. Northern blotting with sense and antisense probes specific for *RMRP* (nucleotides 21–40) identified 22-nucleotide, double-stranded RNAs that contained a 5′ monophosphate and a 3′ hydroxyl group, which were loaded into human AGO2. To determine the function of these *RMRP*-derived small RNAs, a chemically synthesized siRNA corresponding to these small RNAs (siRNA: 5′-GGCTACACACTGAGGACTC-3′; Dharmacon) was transfected into HeLa, 293T and MCF7 cells.

Full Methods and any associated references are available in the online version of the paper at www.nature.com/nature.

Received 28 May; accepted 10 July 2009.
Published online 23 August 2009.

1. Cohen, S. B. *et al.* Protein composition of catalytically active human telomerase from immortal cells. *Science* 315, 1850–1853 (2007).
2. Fu, D. & Collins, K. Purification of human telomerase complexes identifies factors involved in telomerase biogenesis and telomere length regulation. *Mol. Cell* 28, 773–785 (2007).
3. Venteicher, A. S., Meng, Z., Mason, P. J., Veenstra, T. D. & Artandi, S. E. Identification of ATPases pontin and reptin as telomerase components essential for holoenzyme assembly. *Cell* 132, 945–971 (2008).
4. Venteicher, A. S. *et al.* A human telomerase holoenzyme protein required for Cajal body localization and telomere synthesis. *Science* 323, 644–648 (2009).
5. Weinrich, S. L. *et al.* Reconstitution of human telomerase with the template RNA component hTR and the catalytic protein subunit hTRT. *Nature Genet.* 17, 498–502 (1997).
6. Chan, S. W. & Blackburn, E. H. New ways not to make ends meet: telomerase, DNA damage proteins and heterochromatin. *Oncogene* 21, 553–563 (2002).
7. Liu, J. M. & Ellis, S. R. Ribosomes and marrow failure: coincidental association or molecular paradigm? *Blood* 107, 4583–4588 (2006).
8. Calado, R. T. & Young, N. S. Telomere maintenance and human bone marrow failure. *Blood* 111, 4446–4455 (2008).
9. Gonzalez-Suarez, E. *et al.* Increased epidermal tumors and increased skin wound healing in transgenic mice overexpressing the catalytic subunit of telomerase, mTERT, in basal keratinocytes. *EMBO J.* 20, 2619–2630 (2001).
10. Artandi, S. E. *et al.* Constitutive telomerase expression promotes mammary carcinomas in aging mice. *Proc. Natl Acad. Sci. USA* 99, 8191–8196 (2002).
11. Masutomi, K. *et al.* The telomerase reverse transcriptase regulates chromatin state and DNA damage responses. *Proc. Natl Acad. Sci. USA* 102, 8222–8227 (2005).
12. Sarin, K. Y. *et al.* Conditional telomerase induction causes proliferation of hair follicle stem cells. *Nature* 436, 1048–1052 (2005).
13. Lee, J. *et al.* TERT promotes cellular and organismal survival independently of telomerase activity. *Oncogene* 27, 3754–3760 (2008).

14. Tollervey, D. & Kiss, T. Function and synthesis of small nucleolar RNAs. *Curr. Opin. Cell Biol.* 9, 337–342 (1997).
15. Ridanpaa, M. *et al.* Mutations in the RNA component of RNase MRP cause a pleiotropic human disease, cartilage-hair hypoplasia. *Cell* 104, 195–203 (2001).
16. Moriarty, T. J., Huard, S., Dupuis, S. & Autexier, C. Functional multimerization of human telomerase requires an RNA interaction domain in the N terminus of the catalytic subunit. *Mol. Cell. Biol.* 22, 1253–1265 (2002).
17. Lue, N. F. *et al.* Telomerase can act as a template- and RNA-independent terminal transferase. *Proc. Natl Acad. Sci. USA* 102, 9778–9783 (2005).
18. Nakamura, T. M. *et al.* Telomerase catalytic subunit homologs from fission yeast and human. *Science* 277, 955–959 (1997).
19. Mourrain, P. *et al. Arabidopsis SGS2* and *SGS3* genes are required for posttranscriptional gene silencing and natural virus resistance. *Cell* 101, 533–542 (2000).
20. Smardon, A. *et al.* EGO-1 is related to RNA-directed RNA polymerase and functions in germ-line development and RNA interference in *C. elegans*. *Curr. Biol.* 10, 169–178 (2000).
21. Lipardi, C., Wei, Q. & Paterson, B. M. RNAi as random degradative PCR: siRNA primers convert mRNA into dsRNAs that are degraded to generate new siRNAs. *Cell* 107, 297–307 (2001).
22. Sijen, T. *et al.* On the role of RNA amplification in dsRNA-triggered gene silencing. *Cell* 107, 465–476 (2001).
23. Makeyev, E. V. & Bamford, D. H. Cellular RNA-dependent RNA polymerase involved in posttranscriptional gene silencing has two distinct activity modes. *Mol. Cell* 10, 1417–1427 (2002).
24. Semler, B. L. & Wimmer, E. *Molecular Biology of Picornaviruses* 255–267 (American Society for Microbiology, 2002).
25. Behrens, S. E., Tomei, L. & De Francesco, R. Identification and properties of the RNA-dependent RNA polymerase of hepatitis C virus. *EMBO J.* 15, 12–22 (1996).
26. Sugiyama, T., Cam, H., Verdel, A., Moazed, D. & Grewal, S. I. RNA-dependent RNA polymerase is an essential component of a self-enforcing loop coupling heterochromatin assembly to siRNA production. *Proc. Natl Acad. Sci. USA* 102, 152–157 (2005).
27. Masutomi, K. *et al.* Telomerase maintains telomere structure in normal human cells. *Cell* 114, 241–253 (2003).
28. Ford, L. P. *et al.* Telomerase can inhibit the recombination-based pathway of telomere maintenance in human cells. *J. Biol. Chem.* 276, 32198–32203 (2001).
29. Pascale, E., Cimino Reale, G. & D'Ambrosio, E. Tumor cells fail to *trans*-induce telomerase in human umbilical vein endothelial cell cultures. *Cancer Res.* 64, 7702–7705 (2004).
30. Won, J., Chang, S., Oh, S. & Kim, T. K. Small-molecule-based identification of dynamic assembly of E2F-pocket protein-histone deacetylase complex for telomerase regulation in human cells. *Proc. Natl Acad. Sci. USA* 101, 11328–11333 (2004).
31. Almeida, R. & Allshire, R. C. RNA silencing and genome regulation. *Trends Cell Biol.* 15, 251–258 (2005).
32. Schwarz, D. S., Hutvagner, G., Haley, B. & Zamore, P. D. Evidence that siRNAs function as guides, not primers, in the *Drosophila* and human RNAi pathways. *Mol. Cell* 10, 537–548 (2002).
33. Schwarz, D. S., Tomari, Y. & Zamore, P. D. The RNA-induced silencing complex is a Mg^{2+}-dependent endonuclease. *Curr. Biol.* 14, 787–791 (2004).
34. Vagin, V. V. *et al.* A distinct small RNA pathway silences selfish genetic elements in the germline. *Science* 313, 320–324 (2006).
35. Nishikura, K. A short primer on RNAi: RNA-directed RNA polymerase acts as a key catalyst. *Cell* 107, 415–418 (2001).
36. Aoki, K., Moriguchi, H., Yoshioka, T., Okawa, K. & Tabara, H. *In vitro* analyses of the production and activity of secondary small interfering RNAs in *C. elegans*. *EMBO J.* 26, 5007–5019 (2007).
37. Gillis, A. J., Schuller, A. P. & Skordalakes, E. Structure of the *Tribolium castaneum* telomerase catalytic subunit TERT. *Nature* 455, 633–637 (2008).
38. Salgado, P. S. *et al.* The structure of an RNAi polymerase links RNA silencing and transcription. *PLoS Biol.* 4, e434 (2006).
39. Tam, O. H. *et al.* Pseudogene-derived small interfering RNAs regulate gene expression in mouse oocytes. *Nature* 453, 534–538 (2008).
40. Watanabe, T. *et al.* Endogenous siRNAs from naturally formed dsRNAs regulate transcripts in mouse oocytes. *Nature* 453, 539–543 (2008).
41. Babiarz, J. E., Ruby, J. G., Wang, Y., Bartel, D. P. & Blelloch, R. Mouse ES cells express endogenous shRNAs, siRNAs, and other Microprocessor-independent, Dicer-dependent small RNAs. *Genes Dev.* 22, 2773–2785 (2008).
42. Yang, N. & Kazazian, H. H. Jr. L1 retrotransposition is suppressed by endogenously encoded small interfering RNAs in human cultured cells. *Nature Struct. Mol. Biol.* 13, 763–771 (2006).
43. Guggenheim, R., Somech, R., Grunebaum, E., Atkinson, A. & Roifman, C. M. Bone marrow transplantation for cartilage-hair-hypoplasia. *Bone Marrow Transplant* 38, 751–756 (2006).
44. Choi, J. *et al.* TERT promotes epithelial proliferation through transcriptional control of a Myc- and Wnt-related developmental program. *PLoS Genet.* 4, e10 (2008).

Supplementary Information is linked to the online version of the paper at www.nature.com/nature.

Acknowledgements We thank T. Sugimura and S. Hirohashi at the National Cancer Center for comments. We also thank H. Siomi, H. Tabara and Y. Tomari for discussions. This work was supported in part by Grant-in-Aid for Young Scientists (A) 19689010 (K.M.) and Grant-in-Aid for Young Scientists (B) 19791141 (Y.M.) from the Ministry of Education, Culture, Sports, Science and Technology, by the Third-Term Comprehensive Control Research for Cancer (K.M.) from the Ministry of Health, Labor, and Welfare, by a Takeda Science Foundation grant (K.M.), the Uehara Memorial Foundation (K.M.), a J&J Focused Funding Award (W.C.H.) and R01 AG23145 from the National Institutes of Health (W.C.H.).

Author Contributions Y.M., M.Y., M.F., N.O., R.P. and V.K. performed experiments. T.L. and Y.H. designed and carried out the bioinformatics analyses of TERT-associated RNAs. Y.M., M.Y., W.C.H. and K.M. designed the experiments and discussed the interpretation of the results. W.C.H. and K.M. cowrote the manuscript.

Author Information Reprints and permissions information is available at www.nature.com/reprints. Correspondence and requests for materials should be addressed to W.C.H. (william_hahn@dfci.harvard.edu) or K.M. (kmasutom@ncc.go.jp).

METHODS

Cell culture and stable expression of TAP–TERT. The human cell lines 293T, MCF7, HeLa, HeLa S3 and VA-13 were maintained in DMEM supplemented with 10% heat-inactivated FBS. BJ fibroblasts were cultured as described[15]. Amphotropic retroviruses were created as described[15,16] using the vectors pWZL-Blast-N-Flag/HA-TERT (for HeLa-S3-TAP–TERT), pBABE-puro or pBABE-puro-TERT. After infection, cells were selected with blasticidin S (10 μg ml^{-1}) for 5 days or with puromycin (2 μg ml^{-1}) for 3 days.

Purification of TERT complexes and cloning of RNAs. HeLa S3 cells (2×10^8) expressing or lacking (control) TAP–TERT were lysed in 5 ml of lysis buffer A (20 mM Tris-HCl, pH 7.4, 150 mM NaCl, 0.5% NP-40, 0.1 mM dithiothreitol (DTT)) and incubated for 30 min on ice. The lysate was then pelleted by centrifugation (16,000*g*) for 20 min at 4 °C. The supernatant was incubated with anti-Flag (M2) antibody-conjugated agarose overnight at 4 °C. The beads were washed three times with lysis buffer A and eluted with 3× Flag peptide (150 ng μl^{-1}). The resulting elution was incubated with Protein A Sepharose beads and an anti-HA antibody (F7; Santa Cruz) for 4 h at 4 °C. The beads were washed three times with lysis buffer A, and RNA was isolated using TRIzol (Invitrogen). RNA samples prepared in this manner were analysed using an Experion capillary electrophoresis device (Bio-Rad) to visualize RNA species. For RNA cloning and the sequencing, the same samples were separated using a 7 M urea/15% polyacrylamide gel, and RNAs recovered from gel were cloned using a small RNA cloning Kit (TaKaRa).

RNA preparation for immunoprecipitation RT–PCR. RNA samples that were prepared from the HeLa S3 cells expressing TAP–TERT as described earlier were also subjected to RT–PCR. For immunoprecipitation of endogenous TERT complexes, cells (1×10^8) were lysed in 600 μl of lysis buffer A, sonicated and pre-cleared with 15 μl of 50% slurry of Protein A Sepharose (Pierce) for 2 h at 4 °C. The pre-cleared total cell lysate was incubated with a rabbit polyclonal anti-TERT antibody (Rockland, 2 μl) for 3 h at 4 °C, followed by incubation with 30 μl of 50% slurry of Protein A Sepharose overnight at 4 °C. After binding, the beads were washed three times for 30 min with lysis buffer A. RNA derived from a single immunoprecipitation was isolated from the Protein A Sepharose using TRIzol (Invitrogen) followed by RT–PCR with primers specific for *TERC*, *RMRP* or *RNase P*. Although other RNAs also co-purified with human TERT (Supplementary Table 1), we failed to confirm the interaction of *Alu* sequences or the 5.8S ribosomal RNA on the Y chromosome with TERT (data not shown).

RT–PCR and quantitative RT–PCR. Either total cellular RNA or RNA from immunoprecipitation was isolated using TRIzol (Invitrogen) and subjected to RT–PCR. The following primers were used: *TERC* (43F, 5′-TCTAACCC TAACTGAGAAGGGCGT-3′ and 163R, 5′-TGCTCTAGAATGAACGGTGGA AGG-3′), *RMRP* (F5, 5′-TGCTGAAGGCCTGTATCCT-3′ and R257, 5′-TGAGAATGAGCCCCGTGT-3′), *RNase P* (F50, 5′-GTCACTCCACTCC CATGTCC-3′ and R318, 5′-AATTGGGTTATGAGGTCCC-3′), and the human β-actin gene (also known as *ACTB*) (5′-CAAGAGATGGCCACGGCTGCT-3′ and 5′-TCCTTCTGCATCCTGTCGGCA-3′). The reverse transcription reaction was performed for 60 min at 42 °C using the recovered RNA, and PCR was immediately performed (22 cycles for 293T cells, and 26 cycles for HeLa cells: 94 °C, 30 s; 60 °C, 30 s; 72 °C, 30 s).

Quantitative RT–PCR (qRT–PCR) was performed with a LightCycler 480 II (Roche) according to the manufacturer's protocols. The expression levels of *RMRP* were detected using the following primers and probe; forward primer, 5′-GAGAGTGCCACGTGCATACG-3′, reverse primer, 5′-CTCAGCGGGATA-CGCTTCTT-3′, VIC-labelled TaqMan MGB probe, 5′-ACGTAGACATT-CCCC-3′. β-actin was used as a reference.

Total *RMRP* was detected using primers (F5, 5′-TGCTGAAGGCC TGTATCCT-3′ and R257, 5′-TGAGAATGAGCCCCGTGT-3′) that amplify both endogenous and ectopically introduced *RMRP*. In Fig. 4a, for VA-13, BJ and MCF7 cells, reverse transcription was performed using random hexamers (GE Healthcare) and ectopically expressed *RMRP* was detected with vector-specific primers (F5, 5′-TGCTGAAGGCCTGTATCCT-3′ and LKO.1-RT, 5′-ACTGCCATTTGTCTCGAGGT-3′). For HeLa cells, reverse transcription was performed with pQC3′ (5′-AAGCGGCTTCGGCCAGTAACGTTA-3′) and PCR was performed with the primers F5 (5′-TGCTGAAGGCCTGTATCCT-3′) and R257 (5′-TGAGAATGAGCCCCGTGT-3′). Northern blotting and qRT–PCR experiments (Supplementary Fig. 14) confirmed that the differences in *RMRP* levels that were observed using the RT–PCR conditions used in Fig. 4a accurately reflect *RMRP* levels. Signal intensity was measured with ImageJ software.

Telomerase activity reconstituted *in vitro* and TRAP assay. *In vitro* reconstitution of telomerase activity (telomere-specific reverse transcriptase activity) was performed as described previously[5]. In brief, recombinant TERT was expressed in the TnT T7-Coupled Reticulocyte Lysate System (Promega) following the manufacturer's instructions. Purified *TERC* or *RMRP* was included in the *in vitro* transcription/translation reactions. The telomeric repeat amplification protocol (TRAP)[15–17] was used to detect telomere-specific reverse transcriptase activity.

Affinity purification of recombinant GST–TERT fusion proteins. GST–TERT–HA, GST–TERT-HT1 and GST–TERT-DN in the pGENKZ expression vector[18] were provided by S. Murakami. Bacteria (BL21-Gold) containing these vectors were plated at 30 °C overnight and then a single colony was picked to inoculate liquid cultures, which were incubated at 37 °C overnight. Thereafter 1 ml of this culture was re-inoculated into 100 ml of Luria-Bertani medium, incubated at 37 °C for 4 h without isopropyl-β-D-thiogalactoside (IPTG) induction, collected by centrifugation, suspended in a lysis buffer (20 mM Tris-HCl, pH 7.4, 150 mM NaCl, 0.5% NP-40, 0.1 mM DTT, 10 mM phenylmethyl sulphonyl fluoride (PMSF), proteinase inhibitor (Nacalai Tesque)) and sonicated twice for 10 s at 4 °C. After centrifugation of the sonicated lysates, the supernatants were passed through DEAE-Sepharose, and the GST-fusion proteins were recovered using glutathione-Sepharose 4B beads. The resin was washed with lysis buffer A at least three times, and the GST-fusion proteins were then eluted with glutathione at 4 °C for 1 h (20 mM glutathione (reduced form)) in elution buffer (50 mM Tris-HCl, pH 8.8, 150 mM NaCl, 0.5% NP-40, 0.1 mM DTT, 10 mM PMSF, proteinase inhibitor (Nacalai Tesque)). Supplementary Fig. 6 shows that wild type and TERT-DN were produced at similar levels using this method and the effects of incubation time and IPTG on yield. The average yield for this method is 500 ng (5 ng μl^{-1}) of active form of TERT from 100 ml culture.

RdRP assay. The affinity purified recombinant GST–TERT fusion protein (10 ng) was incubated with 1 μg of full length *RMRP* RNA or truncated *RMRP* products (*RMRP* 1–200, *RMRP* 1–120 and *RMRP* 1–60 for Fig. 2i) transcribed *in vitro* (SP6) in 200 mM KCl, 50 mM Tris-HCl, pH 8.3, 10 mM DTT, 30 mM $MgCl_2$, 50 μM rATP, 50 μM rGTP, 50 μM rCTP and 2 μCi of [α-^{32}P]UTP at 32 °C for 2 h. To perform the experiments under low salt conditions, 20 μl of 0.2× SSC was then added to adjust final salt concentration to 15 mM NaCl and 1.5 mM sodium citrate, whereas 20 μl of 4× SSC was added to adjust final salt concentration to 300 mM NaCl and 30 mM sodium citrate to achieve high salt conditions. These mixtures were incubated at 37 °C for a further 1 h. Resulting products were treated with proteinase K to stop the reaction and purified with phenol–chloroform. To ensure that RNA products were completely denatured, we performed both conventional formamide treatment (with 95% formamide/20 mM EDTA gel-loading buffer at 95 °C for 5 min) and a further treatment with 1 M de-ionized glyoxal at 65 °C for 15 min.

To analyse double-stranded RNA produced by the TERT–*RMRP* complex, we performed this RdRP assay and treated the products with bacterial RNase III (*E. coli*, Ambion; 50 mM NaCl, 10 mM Tris-HCl, pH 7.9, 1 mM DTT, 10 mM $MgCl_2$) or RNase T1 (Roche; 50 mM Tris-HCl, pH 8.3, 300 mM NaCl and 30 mM sodium citrate).

Northern blotting. Total RNA and small RNAs (<200 nucleotides in length) were isolated using a mirVana miRNA Isolation Kit (Ambion) according to the manufacturer's protocol. Total RNA or small RNA (10 μg) was separated on denaturing polyacrylamide gels, then blotted onto Hybond-N+ membranes (GE Healthcare) using a Trans-Blot SD Semi-Dry Transfer Cell (Bio-Rad). Hybridization was performed in Church buffer (0.5 M $NaHPO_4$, pH 7.2, 1 mM EDTA and 7% SDS) containing 10^6 c.p.m. ml^{-1} of each ^{32}P-labelled probe for 14 h. The membranes were washed in 2× SSC, and the signals were detected by autoradiography.

Identification of short RNA species derived from *RMRP*. Using ten consecutive probes corresponding to the *RMRP* sequence, we found that the small RNAs derived from *RMRP* shown in Figs 4e–g and 5a were detected by probes containing the complementary sequences to nucleotides 21–40 of *RMRP*. To determine the function of these *RMRP*-derived small RNAs, we purchased a chemically synthesized siRNA targeting this 20-nucleotide portion of the *RMRP* sequence (siRNA: 5′-GGCTACACACTGAGGACTC-3′; Dharmacon) and transfected this siRNA into HeLa, 293T and MCF7 cells plated on six-well dishes using Lipofectamine 2000 (Invitrogen) according to the manufacturer's protocol.

RNase protection assay. *RMRP* RNA was transcribed with SP6 RNA polymerase in the presence of [α-^{32}P]UTP using RiboMAX Large Scale RNA Production System (Promega). Total cellular RNA (30 μg) was hybridized overnight at 60 °C with equal amounts of ^{32}P-labelled *RMRP* sense probe. Hybrids were digested with RNase A and RNase T1. The protected fragments were separated by PAGE under denaturing conditions and visualized by autoradiography.

Analysis of the chemical structure of the ends of small RNAs. To determine the phosphorylation status of the termini of small RNAs, 30 μg of small RNA (<200 nucleotides in length) was treated with calf intestinal alkaline phosphatase (CIP; TaKaRa) for 2 h at 37 °C. CIP was inactivated by phenol–chloroform extraction. Part of the CIP-treated RNA was then treated with T4 polynucleotide

kinase (TaKaRa) supplemented with 1 mM ATP for 2 h at 37 °C, and phenol–chloroform extraction was performed. Small RNA (15 μg) was treated with T4 polynucleotide kinase without ATP for 2 h at 37 °C. The reaction was inactivated by phenol–chloroform extraction. After overnight sodium acetate–ethanol precipitation at −20 °C, the treated RNAs were resolved by 20% denaturing polyacrylamide/urea gel electrophoresis and then analysed by northern blotting[42,43].

To further analyse the 3′ end of these small RNAs, we performed oxidation and β-elimination reactions. Specifically, the $NaIO_4$ reaction was performed by adding 20 μg of small RNA in water to 5× borate buffer (148 mM borax and 148 mM boric acid, pH 8.6) and freshly dissolved 200 mM $NaIO_4$ to create a final concentration of 1× borate buffer and 25 mM $NaIO_4$. The mixtures were incubated for 10 min at 20 °C. Glycerol was added to quench remaining $NaIO_4$, and the samples were incubated for a further 10 min at 20 °C. For β-elimination, small RNAs were dried by centrifugation and evaporation and dissolved in 50 μl of 1× borax buffer (30 mM borax, 30 mM boric acid and 50 mM NaOH, pH 9.5) and incubated at 45 °C for 90 min. Nucleic acids were recovered by sodium acetate–ethanol precipitation at −20 °C overnight, and the treated RNAs were resolved by 20% denaturing 7 M urea PAGE and analysed by northern blotting[43].

Stable expression of shRNA. We used the pLKO.1-puro vector and the sequences described below to create shRNA vectors specific for *TERT*, *Dicer* and GFP. These vectors were used to make amphotropic retroviruses and polyclonal cell populations were purified with selection with puromycin (2 μg ml^{-1}). The sequences used for the indicated short hairpin RNAs are shown below where the capitalized letters represent the targeting sequences: *TERT* shRNA1, 5′-GGAAGACAGTGGTGAACTTCCctcgagGGAAGTTCACCACTGTCTTCCttttt-3′ and 5′-aattcaaaaaGGAAGACAGTGGTGAACTTCCctcgagGGAAGTTCACCACTGTCTTCC-3′; *TERT* shRNA2, 5′-GGAACACCAAGAAGTTCATCTctcgagAGATGAACTTCTTGGTGTTCCttttt-3′ and 5′-aattcaaaaaGGAACACCAAGAAGTTCATCTctcgagAGATGAACTTCTTGGTGTTCC-3′. *Dicer* sequences: *Dicer* shRNA1, 5′-GCTCGAAATCTTACGCAAATActcgagTATTTGCGTAAGATTTCGAGCttttg-3′ and 5′-aattcaaaaaGCTCGAAATCTTACGCAAATActcgagTATTTGCGTAAGATTTCGAGC-3′; *Dicer* shRNA2, 5′-CCACACATCTTCAAGACTTAActcgagTTAAGTCTTGAAGATGTGTGGttttg-3′ and 5′-aattcaaaaaCCACACATCTTCAAGACTTAActcgagTTAAGTCTTGAAGATGTGTGG-3′.

Immunoprecipitation of human AGO2 complexes. HeLa or 293T cells were lysed in lysis buffer A and immunoprecipitation was performed using preimmune sera or anti-AGO2 antibodies[49] (provided by H. Siomi and M. C. Siomi). RNA was isolated using TRIzol from the protein A beads and resolved by electrophoresis on 7 M urea 20% PAGE. Small RNAs were detected by northern blotting with an antisense probe, a sense probe derived from nucleotides 21–40 of *RMRP*, or a *miR-16*-specific probe (5′-CGCCAATATTTACGTGCTGCTA-3′).

45. Hahn, W. C. *et al.* Creation of human tumour cells with defined genetic elements. *Nature* 400, 464–468 (1999).
46. Hahn, W. C. *et al.* Inhibition of telomerase limits the growth of human cancer cells. *Nature Med.* 5, 1164–1170 (1999).
47. Kim, N. W. *et al.* Specific association of human telomerase activity with immortal cells and cancer. *Science* 266, 2011–2015 (1994).
48. Yamashita, T. *et al.* RNA-dependent RNA polymerase activity of the soluble recombinant hepatitis C virus NS5B protein truncated at the C-terminal region. *J. Biol. Chem.* 273, 15479–15486 (1998).
49. Azuma-Mukai, A. *et al.* Characterization of endogenous human Argonautes and their miRNA partners in RNA silencing. *Proc. Natl Acad. Sci. USA* 105, 7964–7969 (2008).

MOLECULAR AND CELLULAR BIOLOGY, Apr. 2010, p. 1620–1633 Vol. 30, No. 7
0270-7306/10/$12.00 doi:10.1128/MCB.00810-09

Requirement of ATM for Rapid p53 Phosphorylation at Ser46 without Ser/Thr-Gln Sequences▽

Masami Kodama,[1] Chihiro Otsubo,[1,2] Toru Hirota,[3] Jun Yokota,[2] Masato Enari,[1,2]* and Yoichi Taya[1,4]*

Radiobiology Division, National Cancer Center Research Institute,[1] and Biology Division, National Cancer Center Research Institute,[2] 5-1-1 Tsukiji, Chuo-ku, Tokyo 104-0045, Japan; Cancer Institute, Japanese Foundation for Cancer Research, Koto-ku, Tokyo 135-8550, Japan[3]; and Cancer Science Institute of Singapore, National University of Singapore, Center for Life Sciences, #02-07, 28 Medical Drive, Singapore 117456, Singapore[4]

Received 22 June 2009/Returned for modification 8 August 2009/Accepted 15 January 2010

p53 phosphorylation at Ser46 following DNA damage is important for preferential transactivation of proapoptotic genes. Here, we report that ataxia-telangiectasia mutated (ATM) kinase is responsible for Ser46 phosphorylation of p53 during early-phase response to DNA damage. To elucidate the direct phosphorylation of p53 at Ser46 by ATM, an ATM mutant (ATM-AS) sensitive to ATP analogues was engineered. *In vitro* kinase assays revealed that p53 was phosphorylated at Ser46 by ATM-AS, even when ATP analogues were used as phosphate donors, although this phosphorylation site is not in an SQ motif, a consensus ATM site. Furthermore, Ser46 phosphorylation by ATM was dependent on the N- and C-terminal domains of p53, unlike Ser15 phosphorylation. Immunofluorescence analyses showed that Ser46-phosphorylated p53 was observed as foci in response to DNA damage and colocalized with γ-H2AX or Ser1981-phosphorylated ATM. These results suggest that ATM phosphorylates a noncanonical serine residue on p53 by mechanisms different from those for the phosphorylation of Ser15.

The tumor suppressor protein p53 activates the transcription of numerous target genes involved in cell cycle arrest, apoptosis, and DNA repair (5, 15, 35). Upon various cellular stresses, p53 is phosphorylated and acetylated at multiple sites to activate downstream target genes (13, 31, 36).

Phosphorylation of p53 at Ser15 leads to the dissociation of MDM2, an E3 ubiquitin ligase, from p53 to prevent MDM2-dependent p53 degradation (36). We have previously shown that Ser46 on p53 is phosphorylated following DNA damage and that this phosphorylation contributes to the expression of p53-regulated apoptosis-inducing protein 1 (p53AIP1) (33). Ser46 phosphorylation also contributes to the preferential transactivation of other proapoptotic genes, such as Noxa and PUMA, to prevent tumor formation (18, 27). Although p38 mitogen-activated protein (MAP) kinase, protein kinase C δ (PKCδ), homeodomain-interacting protein kinase 2 (HIPK2), and dual-specificity tyrosine phosphorylation-regulated kinase 2 (DYRK2) have been reported to phosphorylate p53 at Ser46 in response to UV or adriamycin (ADR), a radiomimetic DNA-damaging agent, these enzymes are controversial candidates for direct kinases for Ser46 phosphorylation occurring in early phase (within 1 h) in response to ionizing radiation (IR) (6, 11, 16, 41, 49).

Ataxia-telangiectasia mutated (ATM) is a member of the phosphatidylinositol 3-phosphate kinase (PI3-K) family and is crucial for the initiation of signaling pathways following exposure to IR. Functional defects of the gene encoding ATM cause the human genetic disorder ataxia-telangiectasia (A-T). The major hallmarks of A-T are neurodegeneration, immunodeficiency, genomic instability, and cancer predisposition (26). Following exposure to IR, ATM phosphorylates Ser/Thr-Gln (S/T-Q) sequences on numerous proteins participating in DNA damage responses (29). Among these proteins, p53 phosphorylation at Ser15 is a well-known target of ATM (3, 7, 21).

Here, we found that ATM directly phosphorylates p53 at Ser46 as well as Ser15 and that ATM is required for acute DNA damage response to induce Ser46 phosphorylation. Unlike Ser15 phosphorylation, the Ser46 phosphorylation by ATM requires both proline-rich and C-terminal domains of p53. Furthermore, Ser46-phosphorylated p53 is partially colocalized with IR-activated ATM that is known to localize at DNA double-strand break (DSB) sites. Interestingly, Ser46 phosphorylation by IR-activated ATM is induced within 1 h and ATM is required for early-phase response to DNA damage.

MATERIALS AND METHODS

RNA interference (RNAi) experiments and RT-PCR. For the expression of short hairpin RNA (shRNA), oligonucleotides containing sequences homologous to ATM (5′-GATCCCCAAGCTATCAGAGAAGCTAATAAATTCAAGAGATTTATTAGCTTCTCTGATAGCTTTTTTTGGAAA-3′ and 5′-AGCTTTTCCAAAAAAAGCTATCAGAGAAGCTAATAAATCTCTTGAATTTATTAGCTTCTCTGATAGCTTGGG-3′) or to HIPK2 (5′-GATCCCCGAAAGTACATTTTCAACTGTTCAAGAGACAGTTGAAAATGTACTTTCTTTTTGGAAA-3′ and 5′-AGCTTTTCCAAAAAGAAAGTACATTTTCAACTGTCTCTTGAACAGTTGAAAATGTACTTTCGGG-3′) (10) were synthesized and the duplex oligonucleotide DNA was inserted into the pSUPER.retro vector (Oligoengine) to generate pSR-ATM and pSR-HIPK2, respectively. These plasmids

* Corresponding author. Mailing address for Masato Enari: Biology Division, National Cancer Center Research Institute, 5-1-1 Tsukiji, Chuo-ku, Tokyo 104-0045, Japan. Phone: 81-3-3542-2511. Fax: 81-3-3542-0807. E-mail: menari@ncc.go.jp. Mailing address for Yoichi Taya: Cancer Science Institute of Singapore, Center for Life Sciences #02-07, 28 Medical Drive, National University of Singapore, Singapore 117456, Singapore. Phone: 65-6516-8706. Fax: 65-6873-9664. E-mail: csiyt@nus.edu.sg.

▽ Published ahead of print on 1 February 2010.

were digested to obtain DNA fragments containing the H1 promoter and DNA coding for shRNA, and these DNA fragments were inserted into pLenti6.2/V5-DEST (Invitrogen) to generate pL-shATM and pL-shHIPK2, respectively. Lentiviruses were produced in accordance with the manufacturer's instructions (Invitrogen) and used to infect MCF7 or U2OS cells. To generate stable cell lines, infected cells were selected with blasticidin (Invitrogen). The sequences of primers for reverse transcription-PCR (RT-PCR) were as follows: 5′-GGCCTCAC ATGTGCAAGTTTTC-3′ and 5′-TTGGTAGGTATCAAGGAGGCTC-3′ for HIPK2 and 5′-TCCACAGTCTTCTGGGTGGCAGTGA-3′ and 5′-GGGGAG CCAAAAGGGTCATCATCTC-3′ for glyceraldehyde-3-phosphate dehydrogenase (GAPDH). For experiments with short interfering RNA (siRNA), Allstars negative-control siRNA and Hs_ATM_5_HP validated siRNA were purchased from Qiagen. Sequences of siRNAs and primers for RT-PCR for HIPK2 and DYRK2 are described by Hofmann et al. and Taira et al., respectively (17, 41). For p53 knockdown, siRNA described previously was used (12). Each 100 pmol of siRNA was transfected with HiPerfect transfection reagent (Qiagen) and RNAiMax transfection reagent (Invitrogen) into MCF7 or U2OS cells (2×10^5 cells). At 48 h after transfection, cells were used for assays.

Immunoblotting analysis. To prepare whole-cell lysates, cells were collected and stored at −80°C. The cells were thawed in chilled IP150 buffer (50 mM HEPES [pH 7.0], 150 mM NaCl, 1 mM EDTA, 2.5 mM EGTA, 10% glycerol, 1 mM dithiothreitol [DTT], 1 mM Na_3VO_4, and 5 mM NaF) containing 0.1% NP-40 and a protease inhibitor cocktail consisting of 10 μg/ml pepstatin A, 10 μg/ml antipain, 10 μg/ml chymostatin, 10 μg/ml leupeptin, 10 μg/ml E-64, and 10 μg/ml phenylmethylsulfonyl fluoride (PMSF). The lysates were centrifuged for 15 min in a microcentrifuge at 4°C, and the supernatants were collected and boiled in sodium dodecyl sulfate (SDS) sample buffer. The samples were separated on SDS-PAGE gels and blotted onto Immobilon-P transfer membrane (Millipore). The membranes were blocked with blocking solution containing 5% nonfat dry milk in phosphate-buffered saline (PBS) containing 0.1% Tween 20 (PBS-T) for 1 h at room temperature and then incubated with primary antibodies diluted in Can Get Signal Solution 1 (Toyobo) overnight at 4°C. After three washes with PBS-T, the membranes were incubated for 1 h with secondary antibodies in PBS-T containing 1% nonfat dry milk at room temperature. Immunoblots were visualized by chemiluminescence (Western Lightning; Perkin-Elmer). Anti-ATM antibody (2C1) was purchased from GeneTex, Inc.; anti-p53 antibody (9282), anti-phospho-Ser15-of-p53 antibody (9284), and anti-phospho-Thr68-of-Chk2 antibody (2661) were from Cell Signaling Technology; anti-phospho-Ser1981-of-ATM antibody (10H11.E12) was from Rockland Inc.; anti-glutathione *S*-transferase (anti-GST) antibody (B14) was from Santa Cruz Biotechnology; and anti-FLAG (M2) antibody was from Sigma. Antibodies to phospho-Ser392 of p53 were described previously (28, 33, 40). Anti-phospho-Ser46-of-p53 mouse monoclonal antibody was generated with a synthetic phosphorylated peptide (Lab of Monoclonal Antibody Co., Inc.). Signals from immunoblots were quantified by Multi-gauge v.3.0 (Fujifilm).

Plasmids and purification of recombinant proteins. An expression construct of FLAG-tagged wild-type ATM was a gift from M. Kastan. To construct expression vectors for the mutant ATM, parts of the FLAG-tagged wild-type ATM were mutated using a QuikChange site-directed mutagenesis kit (Stratagene). Cells transiently transfected with constructs were thawed in IP150 buffer supplemented with 0.3% Nonidet P-40, followed by centrifugation. ATM was purified using anti-FLAG M2 agarose (Sigma) and then eluted into IP150 buffer with 3× FLAG peptides (Sigma) after two washes with IP150 buffer with 0.3% Nonidet P-40, two washes with IP500 buffer containing 500 mM NaCl with 0.3% Nonidet P-40, and two washes with IP150 buffer without detergent. For kinase assays using ATM-AS, a series of ATMs, including ATM-WT and ATM-KD, were prepared in IP150 or IP500 supplemented with 0.03% Nonidet P-40. GST fusion proteins were expressed in *Escherichia coli* BL21 cells from pGEX-4T-1 or pGEX-6P-1 vectors (GE Healthcare).

***In vitro* kinase assay.** ATP was purchased from Cell Signaling Technology, and all ATP analogues were from Biolog. *In vitro* kinase assays were performed in kinase buffer (9802) (25 mM Tris-HCl [pH 7.5], 5 mM β-glycerophosphate, 2 mM dithiothreitol, 0.1 mM Na_3VO_4, and 10 mM $MgCl_2$) (Cell Signaling Technology) supplemented with 10 mM $MnCl_2$ and 0.1 mM ATP or ATP analogues, at 30°C for 30 or 60 min. Reactions were stopped by the addition of SDS sample buffer followed by boiling. Reaction products were subjected to immunoblotting.

Confocal immunofluorescent microscopy. Cells were fixed with 3.7% formaldehyde in PBS for 10 min at room temperature, permeabilized with 0.5% Triton X-100 in PBS for 10 min at room temperature, and then blocked with PBS containing 3% bovine serum albumin (BSA) and 0.1% goat serum for 1 h at room temperature. Cells were incubated with primary antibodies overnight at 4°C and then with secondary antibodies (Alexa Fluor 488 goat anti-rabbit IgG or Alexa Fluor 594 goat anti-mouse IgG; Invitrogen) for 1 h at room temperature. Vectashield with DAPI (4′,6-diamidino-2-phenylindole; Vector Laboratories Inc.) was used as the mounting medium. The primary antibodies used for immunostaining were anti-p53 (Ab-6; Calbiochem), anti-phospho-Ser1981 of ATM (10H11.E12; Rockland Inc.), anti-phospho-Ser15 of p53 (40), anti-phospho-Ser46 of p53 (33), anti-phospho-Thr68 of Chk2 (2661; Cell Signaling Technology), anti-phospho-Ser957 of SMC1 (NB100-205; Novus Biologicals), anti-γ-H2AX (JBW103; Upstate Biotechnology Inc.), and anti-PML antibody (PG-M3; Santa Cruz Biotechnology). All primary antibodies were diluted in Can Get Signal A (Toyobo). These immunostained objects were observed under a confocal immunofluorescent microscope using a Zeiss LSM5 Exciter system equipped with Zen software (Carl Zeiss Inc.). For preextraction experiments, cells were extracted with 0.2% Triton X-100 for 3 min at room temperature prior to 3.7% formaldehyde fixation, followed by the same procedures described above. Fluorescence resonance energy transfer (FRET) signals were obtained as described previously (23). In brief, cells were exposed to 488-nm light to excite Alexa Fluor 488 (donor fluorescence) and the emission of Alexa Fluor 568 (acceptor molecules) was scanned to detect FRET.

RESULTS

ATM is required for p53 phosphorylation at Ser46 following exposure to IR but not to UV. It was reported that Ser46 phosphorylation of p53 is abrogated following exposure to IR in A-T lymphoblasts (38). To identify the kinase that phosphorylates p53 at Ser46 in response to IR, we first assessed whether ATM is required for this phosphorylation in other cell lines. Human mammary carcinoma MCF7 cells were infected with lentiviruses encoding a short hairpin RNA (shRNA) against ATM to generate stable cell lines devoid of ATM expression (pL-shATM) (Fig. 1A). The phosphorylation at Ser46 as well as Ser15 (3, 7, 21) was delayed and attenuated in ATM-depleted cells (Fig. 1B). Similar results were obtained using human osteosarcoma U2OS cells depleted of ATM (Fig. 1C and D). On the other hand, downregulation of ATM expression had no effect on phosphorylation at Ser392 of p53 in either MCF7 or U2OS cells (Fig. 1B and D). In contrast, depletion of ATM had little effect on phosphorylation at Ser46 or Ser15 after exposure to UV (Fig. 1E and F). We also performed immunoblotting to assess Ser46 phosphorylation at various doses of IR. Ser46 phosphorylation was obviously detected at a high dose of IR compared to Ser15 phosphorylation, consistent with previous reports (33) (Fig. 2). These findings suggest that ATM is responsible for the phosphorylation of p53 at Ser46 after exposure to IR but not to UV.

ATM phosphorylates p53 at Ser46 *in vitro*. To examine whether ATM associates with kinases that phosphorylate p53 at Ser46, FLAG-tagged ATM transiently expressed in 293T cells was purified by immunoprecipitation with anti-FLAG antibody and used for *in vitro* kinase assays using full-length p53 fused to GST (GST-p53) as a substrate (Fig. 3A). When wild-type ATM (ATM-WT) was mixed with GST-p53, ATM-WT phosphorylated p53 at Ser46 as well as at Ser15, although neither a kinase-dead ATM mutant (ATM-KD) nor eluates from cells transfected with an empty vector (control) produced the same phosphorylation patterns (Fig. 3A). On the other hand, p53 phosphorylation at Ser392 by ATM was not detected, as shown in Fig. 3A. Given that ATM purified from 293T cells contains the kinase activity to phosphorylate p53 at Ser46, similar experiments were carried out using different cell lines, including human lung carcinoma H1299 and MCF7 cells. Recombinant ATM purified from these cells also phosphorylated p53 at Ser46 as well as Ser15 (Fig. 3B and C), suggesting that the Ser46 kinase activity in the immunoprecipitates was

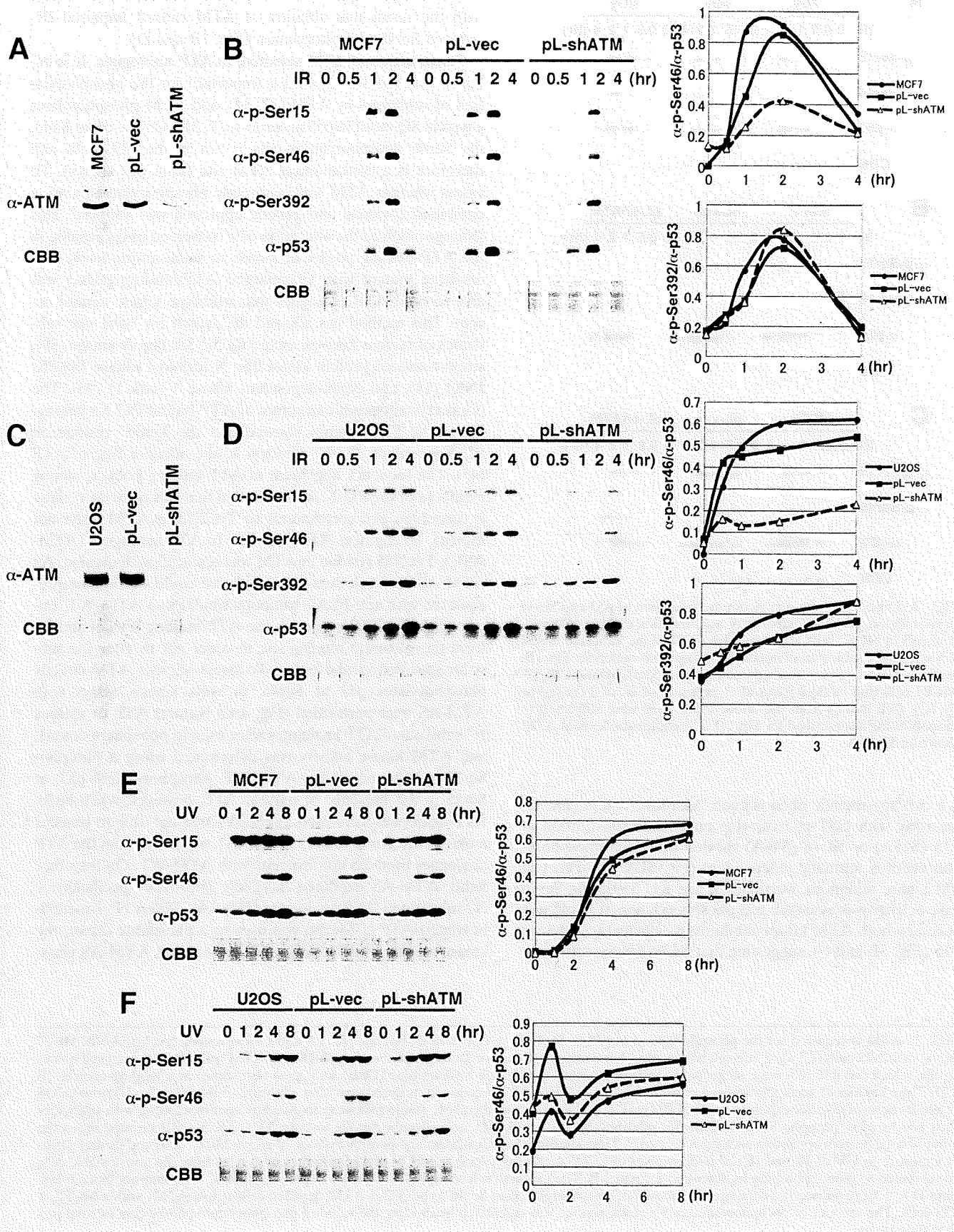

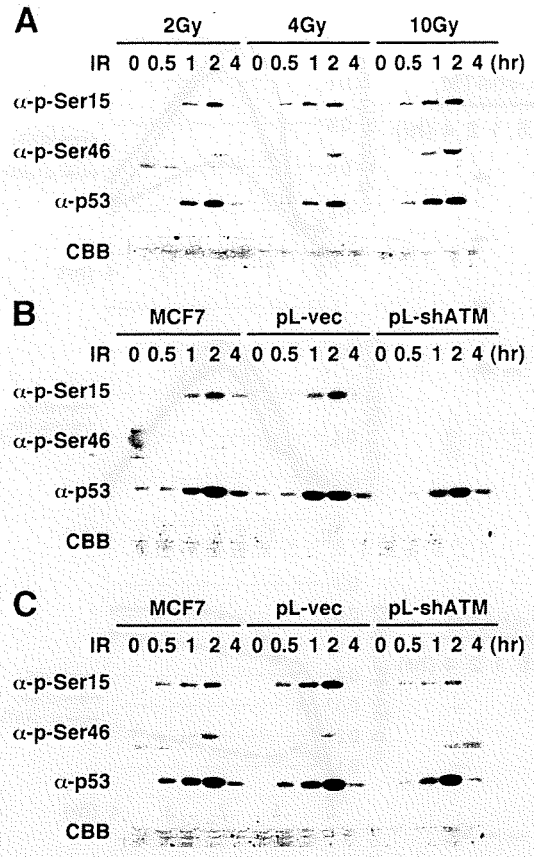

FIG. 2. Dose- and time-dependent accumulation of p53 and Ser46 phosphorylation. (A) Time kinetics of accumulation and phosphorylation of p53 in MCF7 cells after exposure to IR of the indicated doses. Cell lysates were subjected to immunoblotting as described for Fig. 1B. (B and C) Time kinetics of accumulation and phosphorylation of p53 in MCF7 cells and its derivatives after exposure to IR of 2 Gy (B) or 4 Gy (C). Cell lysates from the above stable cells were subjected to immunoblotting as described for Fig. 1B. The expression level of ATM is shown in Fig. 1A.

not a cell-line-specific phenomenon. Moreover, an *in vitro* kinase assay with GST-p53 carrying an alanine substitution at Ser15 (S15A) or Ser46 (S46A) showed that each phosphorylation event is mutually independent (Fig. 3D). The effect of ATM kinase inhibitors, wortmannin and KU-55933, on Ser46 kinase activity was assessed. p53 phosphorylation at Ser46 was blocked by both ATM kinase inhibitors as efficiently as that at Ser15 (Fig. 3E and F), suggesting that Ser46 kinase activity in the immunoprecipitate was dependent on ATM, consistent with the result that ablation of ATM caused impaired IR-induced Ser46 phosphorylation (Fig. 1B and D).

Construction of ATM sensitive to ATP analogues. It is believed that the S/T-Q motif is important for the phosphorylation of substrates by ATM (22, 34), and ATM phosphorylates a typical SQ motif in p53 at Ser15 (3, 7, 21). On the other hand, the Ser46 phosphorylation site is not in the SQ motif and therefore is a noncanonical ATM site (data not shown). To assess whether ATM kinase directly phosphorylates Ser46, a combined chemical and genetic approach was adopted. This strategy involved the alteration of a conserved bulky residue in the ATP-binding pocket of kinase to small amino acids. The resulting mutant with an enlarged ATP-binding pocket was able to bind ATP analogues that wild-type kinase cannot accept. This method has allowed the search for *bona fide* substrates of various kinases, including the Src family kinase (39), stress-activated protein kinase/Jun N-terminal kinase (SAPK/JNK) (14), and cyclin-dependent kinase 1 (cdk 1) (43). The X-ray crystallographic structure of ATP-bound PI3-Kγ belonging to the PI3-K family showed that the Tyr867 residue on PI3-Kγ contacts the N^6 position of the adenine ring of ATP (45). The sequence alignment of ATP-binding pockets among members of the PI3-K family showed that this tyrosine residue is conserved and corresponds to Tyr2755 in ATM (data not shown). To engineer ATM sensitive to ATP analogues (ATM-AS), a Tyr2755 residue in ATM was replaced with alanine. An ATM-AS molecule was expressed and could be immunoprecipitated with anti-FLAG antibody similarly to ATM-WT. Importantly, Tyr2755 is deep in the ATP-binding pocket and far from the substrate binding site in order not to alter the substrate specificity of the kinase. To assess whether ATM directly phosphorylates p53 at Ser46, *in vitro* kinase assays with ATM-AS were performed (Fig. 4A). Natural ATP or various N^6-substituted ATP analogues were used as phosphate donors, and ATM kinase activity was determined using a phospho-Ser15-specific antibody. ATM-WT phosphorylated p53 at Ser15 in the presence of natural ATP; however, when bulky ATP analogues were used, ATM-WT was not able to transfer a phosphate group to Ser15 (Fig. 4A), suggesting that the ATP analogues used did not associate with ATM-WT. On the other hand, ATM-AS exhibited markedly improved specificity for N^6-substituted ATP analogues (Fig. 4A). When N^6-1-methylbutylated-ATP (1-MeBu) was used as a phosphate donor, the kinase activity of ATM-WT was minimal and ATM-AS phos-

FIG. 1. ATM is required for the phosphorylation of p53 at Ser46 in response to IR but not UV. (A and C) Expression level of ATM. MCF7 cells (A) or U2OS cells (C) were infected with control lentiviruses (pL-vec) or lentiviruses encoding shRNA to ATM (pL-shATM), and cell lysates from the selected stable cells were subjected to immunoblotting. Coomassie brilliant blue (CBB) staining is also shown as a loading control. (B and D) Time kinetics of accumulation and phosphorylation of p53 in MCF7 cells and its derivatives after exposure to IR of 10 Gy (B) or in U2OS cells and its derivatives after exposure to IR of 20 Gy (D). Cell lysates from the above stable cells were analyzed by immunoblotting with antibodies against p53 (α-p53), phospho-Ser15 (α-p-Ser15), phospho-Ser46 (α-p-Ser46), and phospho-Ser392 (α-p-Ser392) of p53. CBB staining shows the amount of total protein applied to each lane. (E and F) Time kinetics of accumulation and phosphorylation of p53 in MCF7 cells and its derivatives after exposure to UV of 20 J/m^2 (E) or in derivatives of U2OS cells after exposure to UV of 30 J/m^2 (F). Cell lysates from the above stable cells were subjected to immunoblotting as described for panel B. The expression level of ATM is shown in panels A and C. The immunoblots in Fig. 1B and D to F were scanned to compare the amount of phosphorylation at Ser46 or Ser392 in ATM-depleted cells (pL-shATM) and in MCF7 or U2OS cells. The amount of phosphorylated p53 at each residue was calculated by dividing the value of phosphorylated p53 by that of total p53 at that time point.

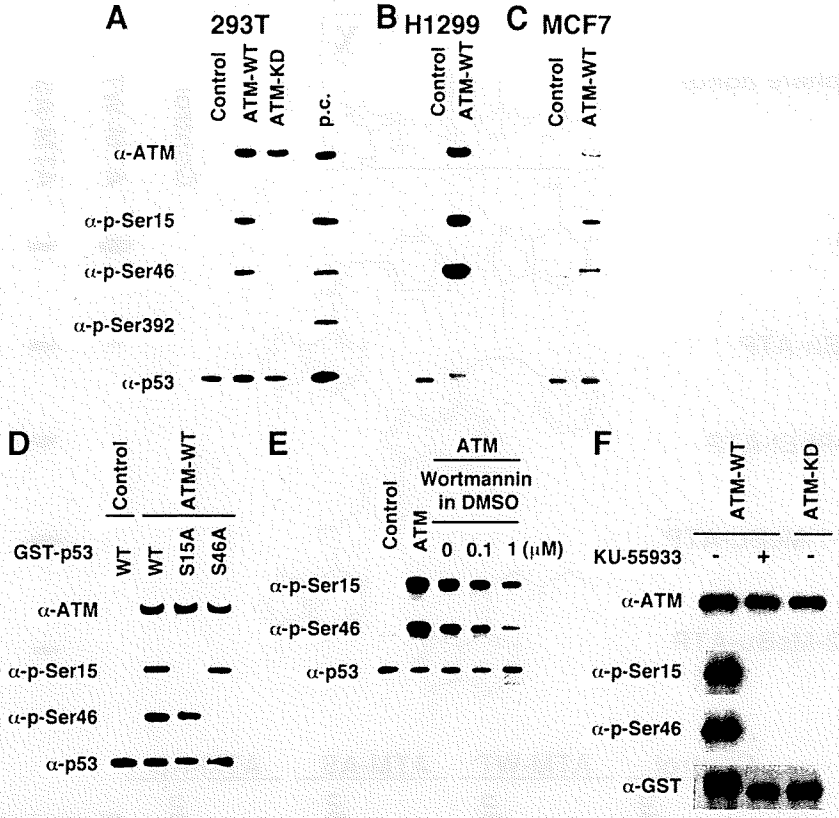

FIG. 3. ATM phosphorylates p53 fused to GST (GST-p53) at Ser46 *in vitro*. (A) Kinase activity of ATM. HEK 293T cells were transiently transfected with an empty vector (control) or an expression construct of FLAG-ATM wild-type (ATM-WT) or kinase-dead ATM (ATM-KD). The kinase activity of ATM purified with an anti-FLAG antibody was analyzed by an *in vitro* kinase assay using GST-p53 as a substrate. Phosphorylated p53 was detected by immunoblotting with the indicated antibodies. ATM in the reaction mixture was also detected by anti-ATM antibody. Cell lysates from MCF7 cells treated with 3 μM ADR are used for positive controls (p.c.) of antibodies. (B and C) Kinase activity of ATM in lysates from different cell lines. H1299 (B) or MCF7 (C) cells were transiently transfected with an empty vector (control) or an expression construct of FLAG-ATM-WT. The kinase activity of ATM purified with an anti-FLAG antibody was analyzed by an *in vitro* kinase assay using GST-p53 as a substrate. Phosphorylated p53 was detected by immunoblotting as described for panel A. (D) GST-p53 carrying an alanine substitution at Ser15 (S15A) or at Ser46 (S46A) was subjected to the *in vitro* kinase assay as in panel A. (E) Effect of an ATM kinase inhibitor on the Ser46 kinase activity of ATM. The *in vitro* kinase assay was performed as in panel A with different concentrations of wortmannin. DMSO, dimethyl sulfoxide. (F) Effect of KU-55933 on the Ser46 kinase activity of ATM. The *in vitro* kinase assay was performed as in panel A with or without 10 μM KU-55933. α, anti.

phorylated p53 at Ser15 more efficiently than ATM-WT (Fig. 4A, row IV).

Kinase domain of ATM directly phosphorylates Ser46 of p53. To explore whether ATM itself directly phosphorylates Ser46 on p53, *in vitro* kinase assays using ATM-AS and N^6-1-MeBu-ATP were performed. If ATM directly phosphorylates Ser46 on p53, ATM-AS would phosphorylate Ser46 as well as Ser15 with N^6-1-MeBu-ATP. If ATM activates a separate Ser46 kinase that is contained in the ATM immune complex, ATM-AS would phosphorylate Ser15 but not Ser46 with N^6-1-MeBu-ATP, as unmodified kinases cannot use ATP analogues as a phosphate donor. The *in vitro* kinase assay revealed that the phosphorylation pattern of Ser46 was quite similar to that of Ser15 (Fig. 4B). ATM-AS phosphorylated both serine residues more efficiently than normal ATP even when N^6-1-MeBu-ATP was used (Fig. 4B, lanes 8 and 9). In contrast, ATM-WT phosphorylated both Ser15 and Ser46 of p53 only in the presence of normal ATP (Fig. 4B, lanes 5 and 6). These phosphorylations were not due to contamination of ATP associated with the immunoprecipitates because the immunoprecipitate complex did not phosphorylate p53 in the absence of phosphate donors (Fig. 4B, lanes 1, 4, 7, and 10). These findings suggest that ATM itself directly phosphorylates Ser46 without any effector kinase.

ATM requires N- and C-terminal domains of p53 for Ser46 phosphorylation. To investigate how ATM phosphorylates a noncanonical target such as Ser46 on p53, the efficiency of Ser46 phosphorylation was analyzed using various deletion mutants of p53. The consensus sequences required for phosphorylation by ATM were identified using a short peptide library (22, 34). However, there is a possibility that ATM might require the whole structure of substrates for sufficient phosphorylation. Therefore, the phosphorylation efficiency between full-length p53 and a short peptide containing Ser15 or Ser46 was compared to evaluate whether Ser46 phosphorylation is a conformation-dependent event. ATM was able to phosphorylate Ser15 on short peptides as efficiently as full-length p53 (Fig. 5A, left). In contrast, no Ser46 phosphorylation was detected on a short peptide (Fig. 5A, right), indicating that the whole structure of p53 is required for Ser46 phosphorylation.

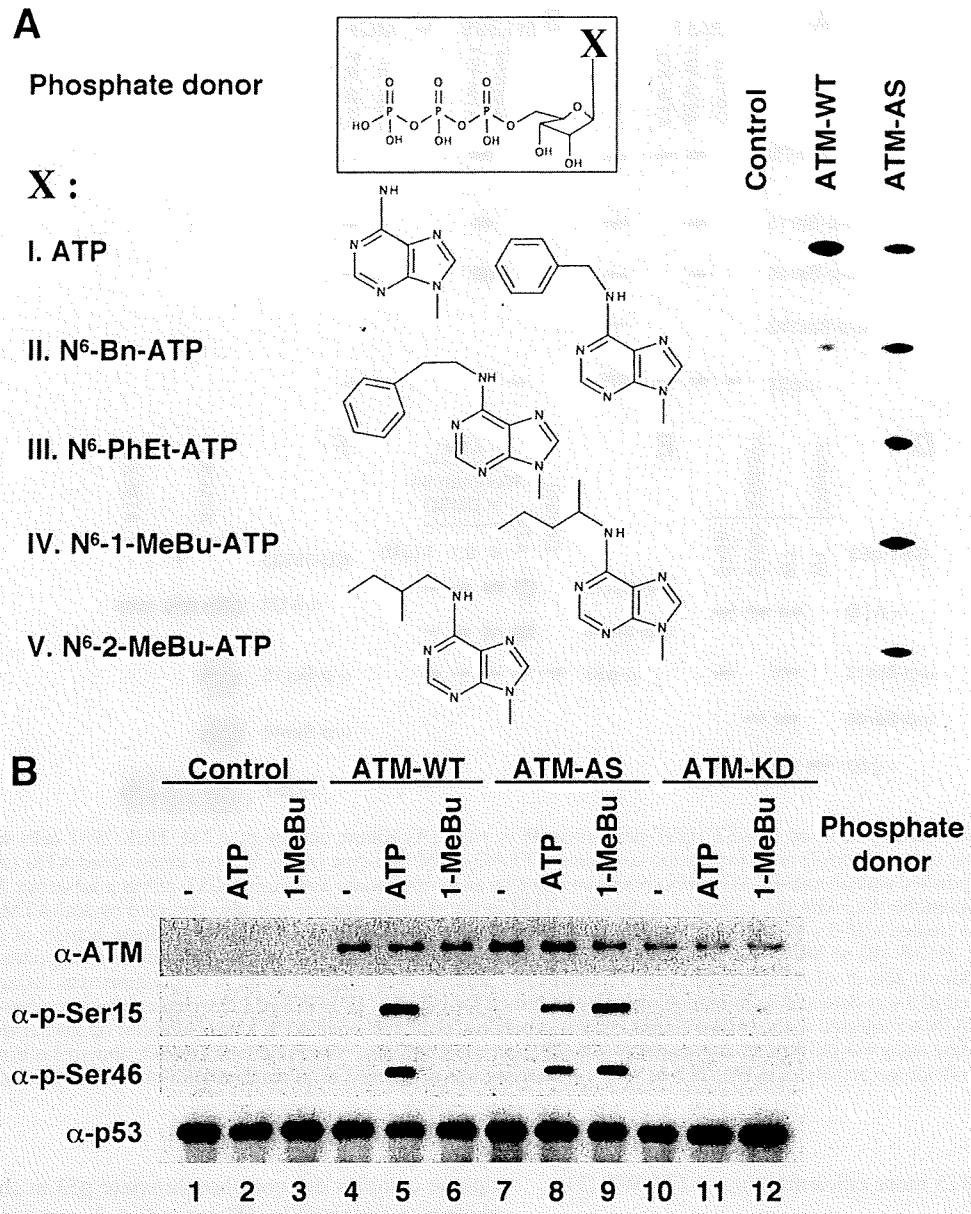

FIG. 4. ATM directly phosphorylates Ser46 of p53 using a mechanism different from that for Ser15. (A) Recombinant ATM was purified from 293T cells expressing FLAG-tagged ATM using anti-FLAG antibody and detected by immunoblotting with anti-ATM antibody. Kinase activity of ATM-WT or an ATM mutant sensitive to ATP analogues (ATM-AS and ATM-Y2755A) was measured by *in vitro* kinase assays using GST-p53. In this assay, natural ATP or various N^6-substituted ATP analogues (row I, ATP; row II, N^6-benzyl ATP [N^6-Bn-ATP]; row III, N^6-phenylethyl ATP [N^6-PhEt-ATP]; row IV, N^6-1-methylbutyl ATP [N^6-1-MeBu-ATP]; row V, N^6-2-methylbutyl ATP [N^6-2-MeBu-ATP]) were used as phosphate donors, and the kinase activity was determined using α-p-Ser15 of p53 antibody. (B) *In vitro* kinase assays of ATM-WT, ATM-AS, and ATM-KD using GST-p53 as the substrate. Immunoprecipitates from 293T cells transfected with empty vector (control) were also subjected to the same assay. ATP or N^6-1-MeBu-ATP (1-MeBu) was used as a phosphate donor for the kinase reaction. "–" indicates a sample without a phosphate donor in the reaction mixture. α, anti.

To exclude the possibility that Ser46 was not exposed because a small region of p53 was fused to a larger GST protein, *in vitro* kinase assays using chemically synthesized p53 peptide were performed (data not shown). Dot blot analysis showed that ATM did not phosphorylate short peptides containing Ser46 without GST (data not shown). Furthermore, antibodies specifically recognized chemically synthesized phosphorylated forms of corresponding short peptides (data not shown). Taken together, these data suggest that the entire p53 structure is required for Ser46 phosphorylation.

To map other regions that may be required for Ser46 phosphorylation, various deletion mutants of p53 were used (Fig. 5B). Deletion of the proline-rich (ΔPro) or C-terminal (ΔC) domains of p53 caused decreased Ser46 phosphorylation *in vitro* (Fig. 5C). In contrast, deletion of the N-terminal TAD1 domain had little or no effect on Ser46 phosphorylation.

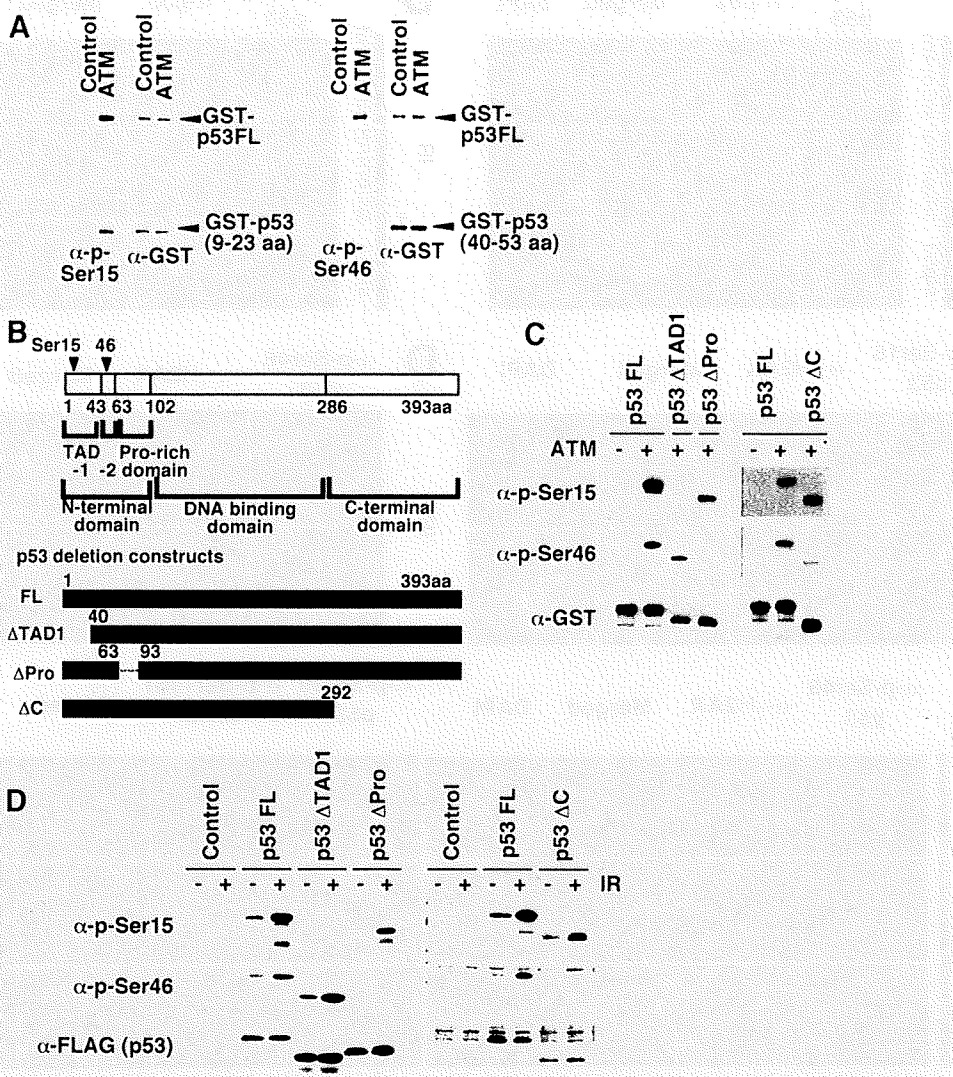

FIG. 5. ATM requires the whole structure of p53 for Ser46 phosphorylation. (A) Comparison experiments of phosphorylation by ATM between p53 full-length and short peptides containing Ser15 (left panel) or Ser46 (right panel) from p53. Full-length p53 and short peptides were produced as GST fusion proteins and used for *in vitro* kinase assay. To compare the phosphorylation efficiencies, full-length p53 and short peptides were mixed and the mixtures were subjected to immunoblotting with indicated antibodies. Specificity of α-p-Ser46 antibody was examined using peptides phosphorylated or not on Ser46 (data not shown). (B) Schematic representation of deletion mutants of p53. Various deletion mutants of p53 were used for the experiments shown in panels C and D. ΔTAD1 corresponds to the deletion of amino acids 1 to 39 of p53, ΔPro corresponds to the deletion of amino acids 64 to 92, and ΔC corresponds to the deletion of amino acids 292 to 393. (C and D) Phosphorylation of p53 deletion mutants *in vitro* (C) or *in vivo* (D). (C) *In vitro* kinase assays using deletion mutants of p53 fused to GST as the substrates. Immunoblotting with anti-GST antibody shows the amount of each substrate in the reaction mixture. (D) Deletion mutants of p53 were transiently expressed in H1299 cells, and at 24 h after transfection, cells were exposed to 0 Gy (−) or 10 Gy (+) of IR. The phosphorylation of p53 at 1 h after IR was detected by immunoblotting. α, anti.

To confirm the effect of the deletion of p53 on Ser46 phosphorylation *in vivo*, the deletion mutants of p53 used for *in vitro* kinase assays were expressed transiently in H1299 cells and the transfected cells were exposed to IR. The proline-rich and C-terminal domains were required for IR-dependent Ser46 phosphorylation (Fig. 5D), which was consistent with *in vitro* data shown above. These findings imply that the whole structure of p53 is required for Ser46 phosphorylation by ATM, although ATM is directed to Ser15 by amino acid sequences surrounding it.

ATM phosphorylates Ser46 of p53 at the sites of DSBs. After exposure to IR, activated ATM is recruited to DSBs and phosphorylates various substrates, including Chk2, SMC1, and H2AX (4, 24, 47). To investigate where ATM phosphorylates Ser46 on p53, antibodies specific for detection of Ser15- and Ser46-phosphorylated p53 were used for immunofluorescence analyses. The specificity of these antibodies was confirmed by immunofluorescence with p53 mutants bearing a mutation at Ser15 or at Ser46 and by immunoblotting with samples from cells with or without DNA damage (data not shown). Following exposure of cells to IR, p53 accumulated in the nuclei (Fig. 6A and B) and Ser15-phosphorylated p53 (Fig. 6A and C) exhibited a diffuse nuclear distribution. On the other hand, confocal immunofluorescent microscopic analyses with an an-

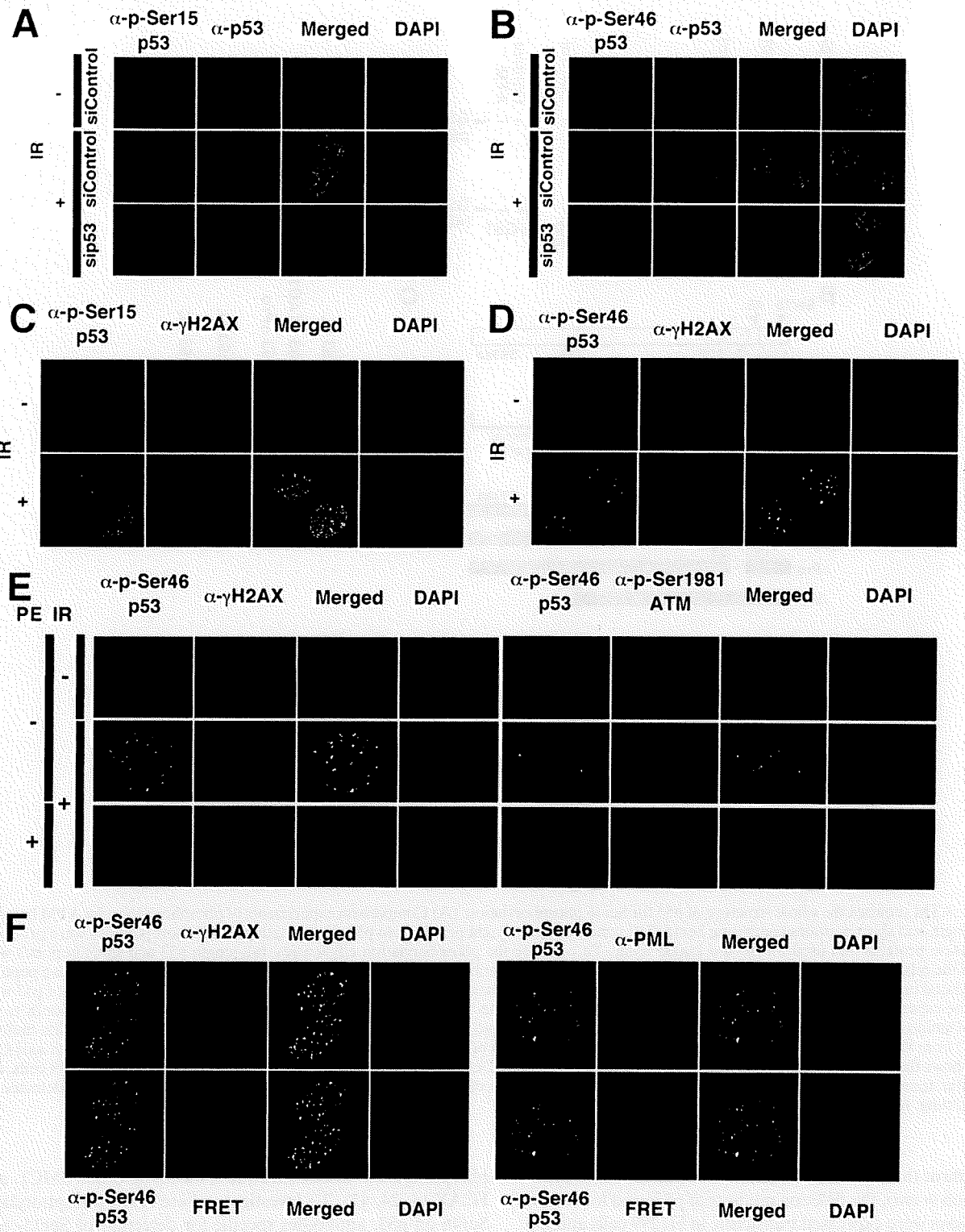

FIG. 6. Ser46, but not Ser15, of p53 is colocalized with activated ATM at DSB sites. (A and B) At 48 h after transfection with either control or p53 siRNA, MCF7 cells were exposed to 0 Gy (−) or 10 Gy (+) of IR and subjected to confocal immunofluorescent analysis at 30 min after irradiation. (A) Immunofluorescence with anti-phospho-Ser15-of-p53 (green) and anti-p53 (red) antibodies. (B) Immunofluorescence with anti-phospho-Ser46-of-p53 (green) and anti-p53 (red) antibodies. (C) Immunofluorescence with anti-phospho-Ser15-of-p53 (green) and anti-γ-H2AX (red) antibodies. (D) Immunofluorescence with anti-phospho-Ser46-of-p53 (green) and anti-γ-H2AX (red) antibodies. (E) Release of Ser46-phosphorylated p53 from chromatin by preextraction of a detergent prior to formaldehyde fixation. MCF7 cells were exposed to 0 Gy (−) or 10 Gy (+) of IR and subjected to confocal immunofluorescent analysis 30 min after irradiation. To assess whether activated ATM (Ser1981-phosphorylated ATM), Ser46-phosphorylated p53, or γ-H2AX is tightly associated with DSB, preextraction (PE) before fixation was performed. (F) Immunofluorescence with anti-phospho-Ser46-of-p53 (green) and anti-γ-H2AX or anti-PML (red) antibodies. Nuclei were stained with DAPI (blue). FRET signals occurring because of colocalization between Ser46-phosphorylated p53 and γ-H2AX or PML are shown (bottom panels).